RENEWABLE ENERGY AND CONSERVATION MEASURES FOR NON-RESIDENTIAL BUILDINGS

By

Andrew James Grossman

A THESIS

Submitted to
Michigan State University
in partial fulfillment of the requirements
for the degree of

Mechanical Engineering – Master of Science

2014

ABSTRACT

RENEWABLE ENERGY AND CONSERVATION MEASURES FOR NON-RESIDENTIAL BUILDINGS

By

Andrew James Grossman

The energy demand in most countries is growing at an alarming rate and identifying economically feasible building retrofit solutions to decrease the need for fossil fuels so as to mitigate their environmental and societal impacts has become imperative. Two approaches are available for identifying feasible retrofit solutions: 1) the implementation of energy conservation measures; and 2) the production of energy from renewable sources. This thesis focuses on the development of retrofit software planning tools for the implementation of solar photovoltaic systems, and lighting system retrofits for mid-Michigan institutional buildings.

The solar planning tool exploits the existing blueprint of a building's rooftop, and via image processing, the layouts of the solar photovoltaic arrays are developed based on the building's geographical location and typical weather patterns. The resulting energy generation of a PV system is estimated and is utilized to determine levelized energy costs.

The lighting system retrofit analysis starts by a current utilization assessment of a building to determine the amount of energy used by the lighting system. Several LED lighting options are evaluated on the basis of color correlation temperature, color rendering index, energy consumption, and financial feasibility, to determine a retrofit solution.

Solar photovoltaic installations in mid-Michigan are not yet financially feasible, but with the anticipated growth and dynamic complexity of the solar photovoltaic market, this solar planning tool is able to assist building proprietors make executive decisions regarding their energy usage. Additionally, a lighting system retrofit is shown to have significant financial and health benefits.

To my Grandpa, Sheridan Norburg, and my parents, Phil and Nancy Grossman, for all of their love and support

ACKNOWLEDGEMENTS

I would like to thank, first and foremost, the students at SPARTA who helped make this possible with all of their hard work and dedication. A special thanks to Kathryn Meersseman for helping me with the edits of countless papers, including this thesis. I would also like to thank my advisors Dr. Richard Lunt and Dr. André Bénard; I could not do it without them. Huge thanks to Dr. Albert Cohen and Tom McCollum for the economic analysis help. Thank you to Dr. Dirk Luchini Colbry for help with the extensive image processing. I would lastly like give a special shout out to beer. Thank you for getting me through graduate school. I owe you.

TABLE OF CONTENTS

LIST OF TABLES

LIST OF FIGURES

Chapter 1 **INTRODUCTION**

The energy demand in many prospering countries is growing at an alarming rate. At the present time, about 80 percent of the world's electricity and heating needs come from fossil fuels such as coal and natural gas. It is well known that these fossil fuels are a large contributor to air pollution, which ultimately leads to the effects of global warming. Nonetheless, these fuels are often times the preferable choice as opposed to renewable sources because of their reliability, present abundance, and well-established extraction and refining techniques. However, unlike solar and wind energy, a finite quantity of fossil fuel exists which makes them vulnerable to market fluctuations. In 2013, about 63 percent or roughly 2.2 trillion barrels of the oil were imported in the United States (US). This equated to about $218 trillion in foreign exchange. The US accounts for 4.5 percent of the world's population yet consumes 25 percent of the global oil production [1].

Nuclear power in the US was attributed to roughly 19.4 percent of the US electricity consumption in 2013. Nuclear power has many advantages such as lower greenhouse gas emissions and high energy density in comparison to conventional fossil fuels. However, the disadvantages of nuclear power include radioactive waste by-products, which poses a threat to human health, potential cataclysmic consequences if system failures occur, and it requires a large amount of water. In March 2011, Japan's Fukushima Daiichi nuclear power plant encountered severe damaged from an earthquake and a tsunami. As a result, the radioactive fallout was not only increased in Japan, but also scientists reported increased radioactivity in the US. The Fukushima nuclear disaster was second largest in history, only behind the 1986 Chernobyl disaster [1, 2].

In regards to energy consumption and the environment, buildings play significant role. For instance, 40 percent of the US's energy consumption is attributed to the nation's 120 million buildings, where 72 percent of that energy is electricity consumption. Furthermore, it is projected that from 2007 to 2025, the total energy consumption due to buildings is expected to increase by 50 percent. The main reason behind this growth is that new buildings are being constructed

before old buildings are retired. Given this expected growth, along with the finite quantities of fossil fuel available, brings about the possibility of an energy paradigm. Therefore, identifying economically feasible building retrofit solutions that decrease the need for fossil fuels has become imperative [3, 4].

The United States Department of Energy (DOE) defines retrofit as a process of improving and/or upgrading a building's infrastructure such that significant energy cost savings are achieved. Typically, a building retrofit is separated in two categories: 1) energy conservation measures, and 2) energy production by means of renewable sources [3]. Accordingly, the focus of this thesis is separated into two sections, where the first section focuses on the development of a solar photovoltaic (PV) planning tool that takes a ubiquitous approach towards utilizing rooftops, while the focal point of the second section presents a methodology for analyzing a lighting system retrofit while working on a limited budget.

The next chapter will give an overview of the basic PV characteristics, as well as an examination of the current PV system modeling tools. The subsequent section discusses a design methodology for developing a PV planning, which is tested and verified on two case studies. The last chapter will discuss a method for a lighting system retrofit.

Chapter 2 **PHOTOVOLTAIC OVERVIEW**

The intent of this chapter is to provide a brief overview of solar photovoltaics. It begins with a discussion regarding its history, which is followed by a summary of the PV effect in a single-junction solar cell. Next, the performance parameters of a solar cell are reviewed, along with the common PV technologies. The subsequent sections present a compendium of PV systems and modeling tools, which is concluded by a summary of the PV market.

2.1 Solar Photovoltaic History

Since the 7th century, people have investigated techniques for harnessing and converting solar energy into useful applications. Initial applications entailed creating fire by concentrating the sun's energy via glass and mirrors. Today, solar energy is still utilized to light fires, but since the discovery of the PV effect in 1839, by French physicist Edmond Becquerel (1820-1891), solar energy is used for an assortment of applications ranging from charging an iPod to powering vehicles and buildings. When Becquerel was 19, he recognized that when two electrodes are exposed to light, electricity is generated, where the amount generated is proportional to the sun intensity. His experimental setup consisted of a black box that contained an acidic solution and housed the electrodes that were either coated with AgCl or AgBr [5, 6]. In 1887, Heinrich Hertz (1857-1894) discovered that ultraviolet light influences the lowest voltage capable of inducing a spark to jump between two electrodes [7]. However, the PV effect remained an anomaly of the science community for the next three quarters of a century. Through the 1940s and 1950s, research was conducted to develop a process that will create highly pure crystalline silicon. This process is known as the Czochralski process, which led to the cultivation of commercializing PV cells. In 1954, Scientists at Bell Laboratories depended on the Czochralski process to develop a crystalline silicon PV cell, with an efficiency of six percent [7]. Today, the main research focus for solar cells are crystalline silicon, thin-film, multi-junction, organic and dye-sensitized [5, 6].

2.2 Solar Cells and the Photovoltaic Effect

The PV effect, depicted in Figure 2.1, is the physical process by which a solar cell converts sunlight into electricity. The semiconductor of a silicon solar cell consists of mainly two layers, n-type layer and p-type layer, and the barrier where these two layers meet is the pn junction. The n-type layer is negatively charged and is formed by doping with impurity atoms that have an excess valence electron, which is typically phosphorous. The p-type layer is positively charged and is formed by doping with impurity atoms that have one less valence electron, which is typically boron [8, 9].

When sunlight collides with the silicon solar cell, one of three things may occur: 1) the photon passes right through the silicon, 2) the photon is reflected at the surface of the silicon, or 3) the photon is absorbed by the silicon. If the photon is absorbed and has enough energy to free an electron, the negative electron charge flows from the n-type layer, via an external electric circuit, to a load such as a light bulb and then to the p-type layer, where they recombine with holes. This flow of electrons is how the electrical current is produced within the solar cell. The charge separation between the n and p-type layer at the junction creates a voltage, which drives the current through the external circuit [8, 9].

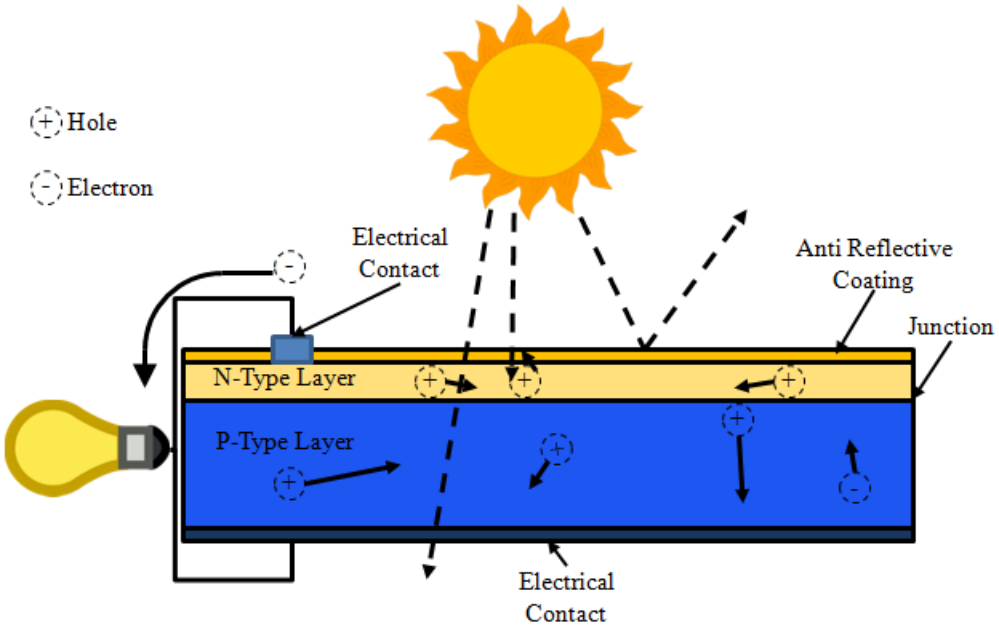

Figure 2.1. The light that encounters the cell creates electron-hole pairs, which are separated by p and n-type layer barrier, thus creating a voltage that moves a current through an external circuit. For interpretation of the references to color in this and all other figures, the reader is referred to the electron version of this thesis.

2.3 Performance of Solar Cell

The maximum power point, fill factor, and efficiency of a solar cell are influenced by a copious amount of factors during conversion. These factors are often the result of many climatic conditions such as irradiance, ambient temperature, snow, wind, and dust.

2.3.1 Maximum Power Point

Figure 2.2 depicts a typical current-voltage (I-V) and power-voltage (P-V) curve for a solar cell, where at the "knee" of the curve denotes a solar cells maximum power point P_{mp}. This is found by multiplying both the short circuit current at the maximum power point I_{mp} with the voltage at the maximum power point V_{mp}. The electric output of a module is dependent upon the module efficiency and technology [10].

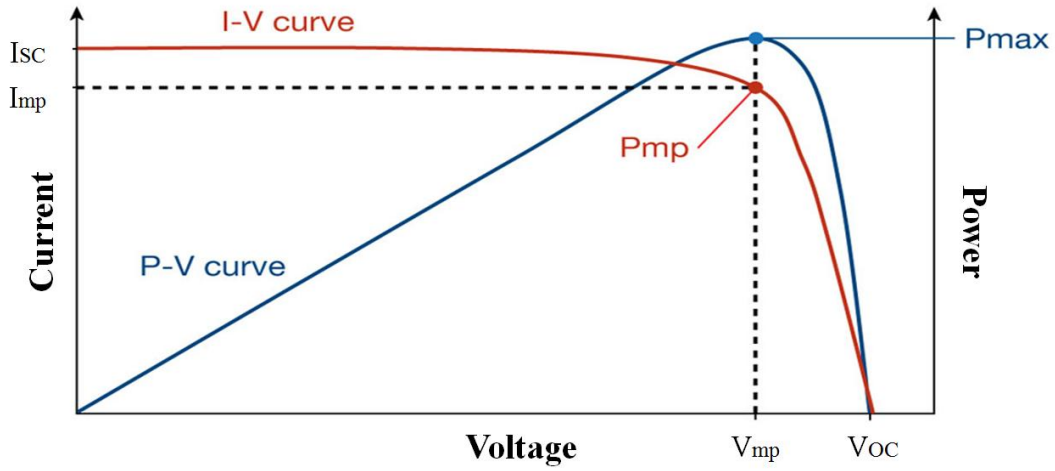

Figure 2.2. Typical I-V and P-V curve, as well as the key points of these curves for a solar cell [10]

2.3.2 Module Efficiency

The efficiency of a PV cell η_{PV} is defined as the ratio of the energy output from the solar PV cell with respect to the solar global irradiance G at standard testing conditions (STC) entering the cell, i.e.

$$\eta_{PV} = \frac{I_{mp} \cdot V_{mp}}{G \cdot A} \tag{1}$$

where A is the is the area of the solar PV cell. The STC are an irradiance 1000 W/m^2, an air mass (AM) of 1.5 spectral distribution, and a 25˚C solar PV cell temperature. The efficiency is a vital performance factor for the situation when space is limited and a certain amount of power is needed [8].

2.3.3 Fill Factor

Figure 2.3 depicts I-V curve, where the fill factor *FF* is the green area. The fill factor is defined as a ratio of the maximum power of the solar cell to the product of the open circuit voltage V_{OC} and short circuit current I_{SC}, in other words

$$FF = \frac{I_{mp} \cdot V_{mp}}{I_{SC} \cdot V_{OC}} \tag{2}$$

An ideal solar cell would produce a perfectly rectangular I-V curve, where the short circuit current and open circuit voltage coincide with the current and voltage at the maximum power point. The importance of the *FF* is it's comparative abilities. If comparing two solar cells with the same I_{SC} and V_{OC}, the module with the higher *FF* will produce more power [10].

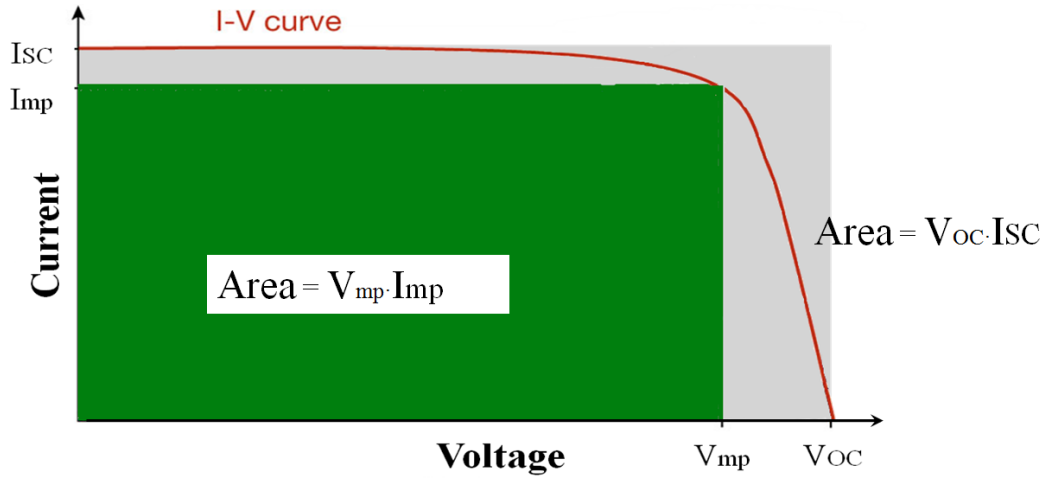

Figure 2.3. The fill factor, defined by the green area and divided by the gray area [10]

2.3.4 Temperature Effect

Figure 2.4 depicts how the ambient temperature affects a solar cell's performance. When the ambient temperature is greater than the STC temperature, 25˚C, the short circuit current slightly increases, whereas the open circuit voltage is dramatically reduced. In other words, the current increase is proportional to a voltage decrease. Overall, when the temperature is above the STC temperature, the overall power output of the module is reduced [11].

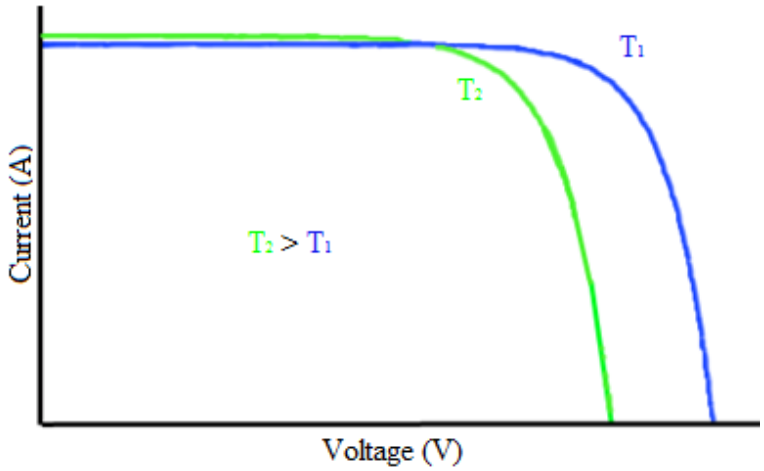

Figure 2.4. The effects of the ambient temperature on a solar cell's current and voltage [10]

2.3.5 Irradiance Effect

Figure 2.5 depicts how the solar irradiance affects a solar cell's current and voltage. The short circuit current of a solar cell is linearly proportional to irradiance, whereas the open circuit voltage of a PV module is logarithmic with respect to irradiance [11].

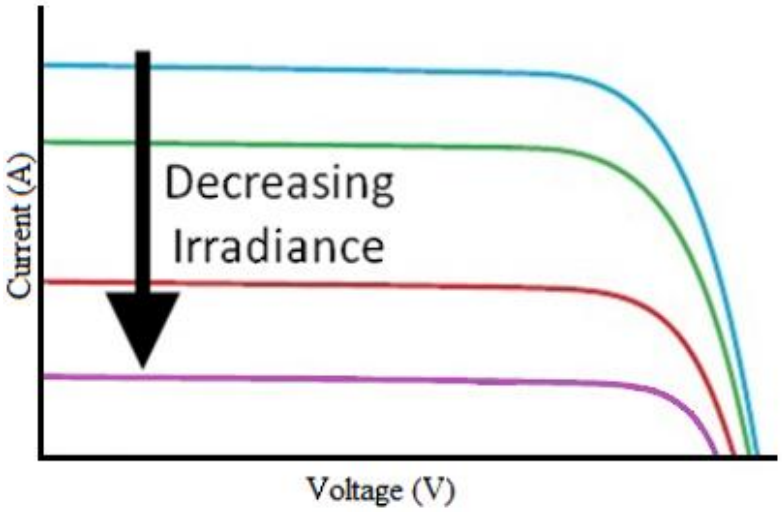

Figure 2.5. The effects of the solar irradiance on a solar cell's current and voltage [10]

2.3.6 Optical Loss

There are two main types of irradiation that can enter a solar cell, direct and diffuse, where direct irradiance is mainly responsible for generating power. The diffuse irradiance is less intense compared to the direct irradiance because it encounters obstructions or absorptions before

reaching the module. Some of these obstructions may be due to atmospheric conditions, surrounding landscape features, while other obstructions or absorptions may be due to the module's glass cover, anti-reflective solar cell coating layers or ethyl vinyl acetate encapsulant [12].

2.3.7 Degradation

The main cause of a PV module degrading overtime is due to UV radiation diminishing the ethyl vinyl acetate encapsulant and the back sheet layers. These layers are discussed in Section 2.4.

Figure 2.6. The brown area of the PV cell is caused by UV radiation degrading the ethyl vinyl acetate layer [12]

The UV radiation causes these materials to lose elasticity, and results in moisture reaching the PV cells. This moisture causes an electrical resistance within the connections, and thus, the output voltage and current decreases. Other degradation factors include lamination disintegration of the backing material, solder-joint wear, hot spots, and discoloration as depicted in Figure 2.6. NREL has classified degradation into five categories:

1. Degradation of packing materials
2. Degradation of cell/module interconnects
3. Degradation caused by moisture intrusion
4. Degradation of the semiconductor device
5. Loss of adhesion

Further, the degradation of a PV module differs by the type of technology and region, depending on the climate and weather. Overall, crystalline silicon has an average annual module degradation rate of 0.36-0.64% and the degradation of the entire PV system ranges from 0.23-0.90%, where a breakdown is shown Table 2.1 [12, 13].

Table 2.1. Overall crystalline silicon degradation rate per year

Technology	Configuration	Degradation Rate per Year
Monocrystalline technology	Module	0.36-0.47%
	System	0.23-0.90%
Polycrystalline Technology	Module	0.61-0.64%
	System	0.59-0.60%

2.3.8 Dirt, Dust, Snow, and Wind

Typically, wind increases the performance of a PV module because the convection reduces the operating cell temperature. However, dirt, dust and snow can cause optical losses and partial shading. When a module experiences partial shading, the shaded modules act as a load by consuming the power from other modules. This load consumption causes harmful excessive heat, which results in failure before the expected lifetime [14]. On the other hand, if the module is not covered with snow, the diffuse solar energy may reflect of the surrounding snow, which may cause more irradiance entering the module, thus increasing the energy production [13, 15].

2.4 Common Photovoltaic Technologies

Although a substantial amount of research is currently being performed on a multitude of PV technologies, as portrayed in Figure 2.7, the single junction PV technology is currently the most cost effective, and accounted for 87% of the global PV market sales in 2011 [16].

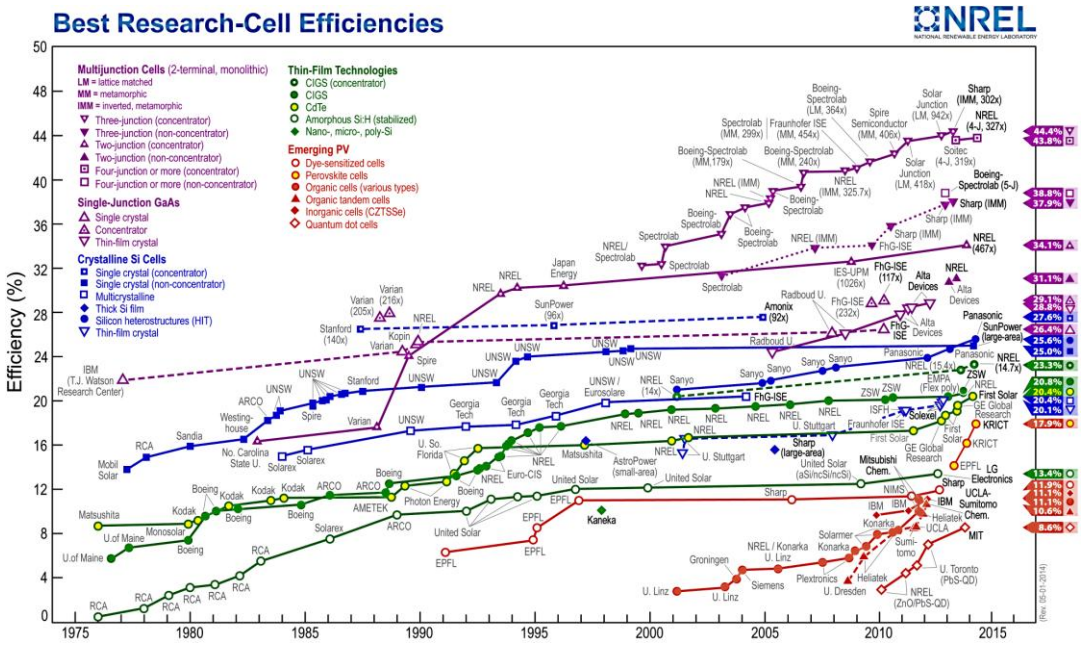

Figure 2.7. Various solar cell technologies and their respective record for efficiency [17]

The main layers of a single junction PV module are depicted in Figure 2.8. The front surface the module is primarily low iron glass. This type of glass is used because it has low reflectivity, high transmissivity, and self-cleaning properties, as well as its impermeability to water and gas, and it is relatively inexpensive. The next layer is a transparent ethyl vinyl acetate film that encapsulates the solar cells within the module. This film is used because its properties have a strong bond to the solar cells and it is stable at different operating temperatures. The back surface is a thin polymer sheet, typically tedlar. Tedlar is used because its properties have low thermal resistivity and low water/water vapor permeability. The solar cells, which was described in Section 2.2, are responsible for producing power [18].

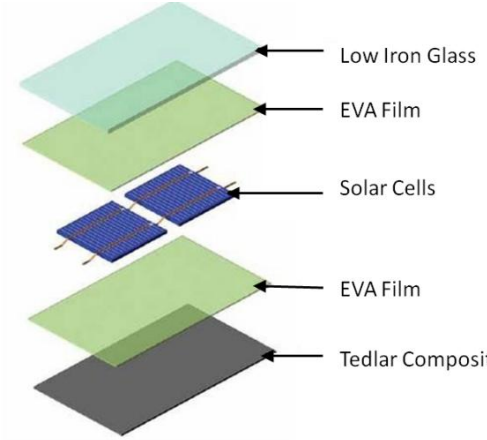

Figure 2.8. Single junction PV module Layers[10]

2.4.1 Crystalline Silicon Technology

Crystalline silicon PV cells have many benefits including being the highest rated efficiency in comparison to other single pn junction modules on the market. Additionally, silicon is a very abundant element, and because this is a mature technology, a considerable amount of research has been performed regarding its reliability and robust design [19, 20].

2.4.1.1 Monocrystalline Silicon Technology

Of all the crystalline silicon solar cell technologies on the market, monocrystalline is not only the oldest, but is also the most efficient with an average efficiency range of 16-18%, and a maximum reported efficency of 25% [20]. The solar cell has a thickness of about 0.2-0.3 mm, and has many shapes such as round, semi-round, and square. The square cells offer the highest packing density in the module but are the most expensive, whereas round cells are the cheapest because less material is wasted during production. The color of cell is either black if it contains an anti-reflective coating, shown in Figure 2.9, or gray if it does not contain an anti-reflective coating [19, 20].

Figure 2.9. Monocrystalline solar cell [20]

2.4.1.2 Polycrystalline Silicon Technology

Polycrystalline solar cells were developed as a means to reduce production costs, and in 2008, they accounted for 48% of the world's solar cell production. The silicon wafers within the module are fabricated ingots, which were casted from molten silicon. Polycrystalline silicon PV technologies have a typical efficiency range of 15-17%, but have been proven to be as efficient as 20.4% [20]. The color of

cell is either bluish-black, if it contains an anti-reflective coating, shown in Figure 2.10, or can be green, gold, silver, brown, or violet if it does not contain an anti-reflective coating [19, 20].

Figure 2.10. Polycrystalline solar cell [20]

2.4.2 Thin Film Technology

Over the last few years, thin film technology has received a considerable amount of attention due to its wide range of applications, aesthetic qualities, and functional value. The 2011-2016 market predictions anticipate an annual growth of 27.5%, which may be associated with the fact that this technology requires less energy and production materials to manufacture them in comparison to crystalline technology, thus making them cheaper [21, 22].

There are many attributes regarding thin film photovoltaics. For instance, this technology can be utilized on any surface, including curved surfaces, because it can be deposited on flexible substrates. The common applications are roof shingles and calculators, as well as less common applications, such as windows, metal, plastic and paper [22]. Another notable quality is that this technology can be designed for specific angle dependence properties that increase the responsivity at off-normal solar incidence angles. Furthermore, thin film photovoltaics experience a performance increase at high ambient temperatures, whereas crystalline technology encounters a performance decrease [22].

The typical semiconductor materials are amorphous and microform silicon (a-si and μ-si), cadmium telluride (CdTe), and copper indium selenide and copper indium gallium selenide (CIS and CIGS) [22].

2.4.2.1 Amorphous and Microform Silicon Technology

Amorphous and microform silicon technology is the first thin technology, and commonly used in small electronic devices such as hand-held calculators. Unlike traditional bulk-crystalline silicon technology, the silicon atoms are in a non-order arrangement and the active material is 1/300th of the thickness. However, the efficiency of amorphous and microform silicon ranges from 12 to 13%, and they have a shorter lifetime in comparison to crystalline silicon technology [22, 23]. The layer structure of an amorphous solar cell is shown in Figure 2.11, where the transparent conducting oxide is usually SnO_2.

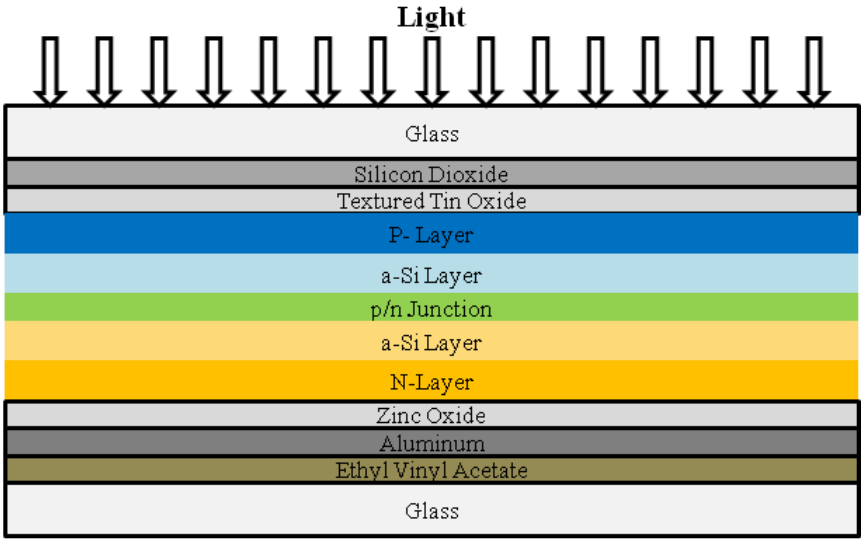

Figure 2.11. Layer structure of an amorphous solar cell deposited on a glass substrate [18, 24]

2.4.2.2 Cadmium Telluride Technology

Cadmium telluride technology is the first and only thin film technology that surpasses crystalline technology in price per watt peak, and is the second most widely used solar cell material. The highest efficiency reported has been 20.4 percent, whereas the typical efficiency ranges from 9 to 11% [22]. Although cadmium telluride technology is known for its ease of manufacturing and efficiency, there are many drawbacks that hinder large-scale commercialization. For instance, cadmium is an abundant but toxic element, which consequently affects the disposal and long-term safety. Furthermore, tellurium is a rare earth element [22, 23]. The layer structure of cadmium telluride solar cell in depicted in Figure 2.12.

Figure 2.12. Layer structure of a cadmium telluride solar cell [18, 24]

2.4.2.3 Copper Indium Selenium Technology

Copper indium selenium technology is the most efficient thin film solar cell at 20.8%, which is partially due to it having a relatively high responsivity at low and indirect sun light [22]. In comparison, crystalline silicon technology has better heat resistance, and unlike cadmium telluride technology, this technology does not require any toxic materials. In regards to large-scale commercialization, the copper indium selenium technology materials are much more difficult to manufacture, thus hindering its introduction into the general market [22, 23]. Figure 2.13 shows the layer structure of a copper indium gallium selenide solar cell.

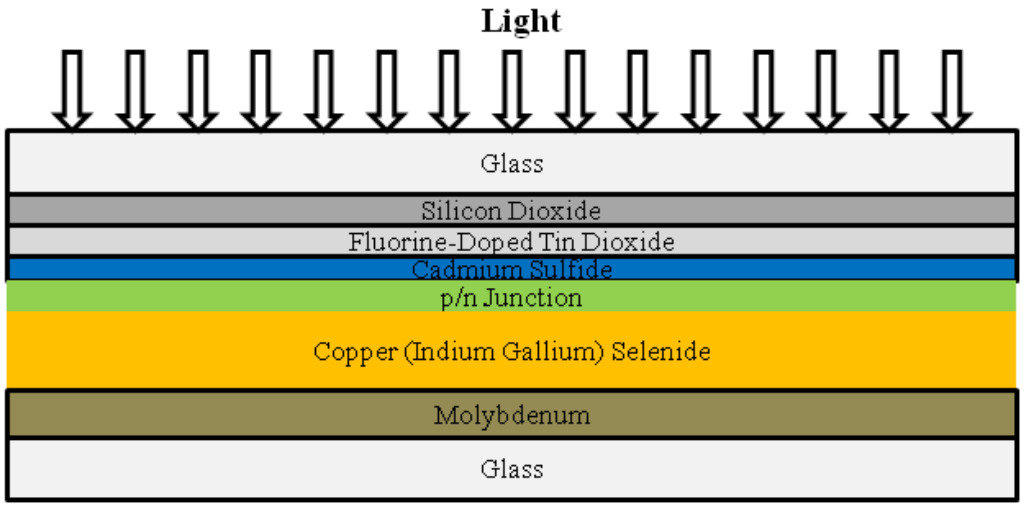

Figure 2.13. Layer structure of a copper indium gallium selenide solar cell [18, 24]

2.5 Photovoltaic Systems

There are two main types of PV systems: 1) off-grid and 2) grid-tied. Off-grid PV systems are typically installed in remote areas and are a stand-alone source of electrical energy. In addition, off-grid PV systems can be coupled with another energy source such as wind or a diesel generator, which is known as a hybrid system. Grid-tied PV systems are connected to the utility power distribution and may be used to supply power to the utility power grid or supplement the utility power needs of the building. Furthermore, grid-tied PV systems have the advantage of lower capital cost because these systems avoid the need for energy storage components. In addition, avoiding the need for energy storage components eliminates energy storage losses, thus making grid-tied PV systems more effective [8, 18, 24, 25].

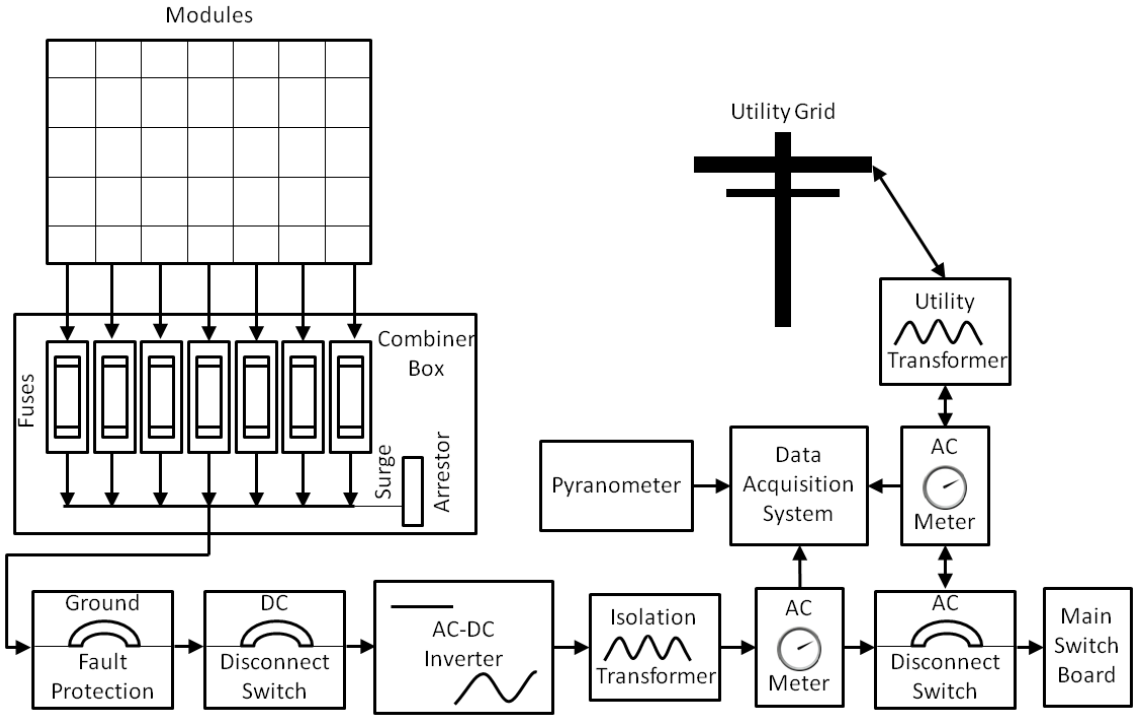

Figure 2.14. Components of a grid-tied PV system, coupled with the power flow

In Figure 2.14, the typical components of a grid-tied PV system are shown, along with arrows indicating the direction of the power flow. A PV module is comprised of solar cells connected in series to build voltage and modules are further connected in series and parallel connections. The characteristic properties of a module depend on the type and quantity of solar cells, and how the solar cells are electrically connected. In a conventional PV system, modules are connected in series to form strings, such

that the operating voltage of the system is increased. The power produced from the strings is transmitted through fuses to a power inverter. Combiner boxes are typically used to converge the power from the strings onto a single interconnection to consolidate wiring. In doing so, the current from the system is increased based on the amount of strings entering/exiting the combiner box. An inverter converts the DC power of the modules into AC power, which is then transmitted to the power grid, or load application [8, 18, 24, 25]. This is further explained in Chapter 3.

2.6 Review of Photovoltaic Modeling Tools

Designing and simulating a solar PV system is rather straightforward. Energy flows from the modules, through a series of components, to the source needing power. Currently, numerous software tools are available for analyzing and dimensioning a PV system. These software packages range from exceptionally basic to exceedingly sophisticated, and may be classified into three categories: 1) pre-feasibility, 2) sizing, and 3) simulation [26, 27].

This section presents an overview of the software tools that are currently available on the market, however, because there are a large number of tools, this list is not exhaustive, the tools are not ranked or rated, but distinguishing attributes are noted.

2.6.1 Pre-Feasibility Tools

A pre-feasibility tool, such as FATE2-P and RETScreen, automates calculations that typically an engineer would do by hand. The main attribute of these tools is their ability to perform a first time assessment at a specified location for possible energy generation and levelized cost of energy. Often times, these tools are implemented as spreadsheets, because minimal iterative work is required and calculations may be automated. Advanced pre-feasibility tools have macros or code embedded within the spreadsheet to provide a more detailed analysis. Generally, energy planners, financiers, vendors, and other people who need a quick evaluation use these tools [26, 27].

2.6.1.1 Financial Analysis Tool for Electrical Energy Projects (FATE2-P)

FATE2-P is a financial analysis spreadsheet based tool, developed by NREL and Princeton Economic Research Inc. This tool has the ability to take into account financial consideration such as debt, tax credits and government incentives [26, 27, 28].

2.6.1.2 RETScreen International

RETScreen International is a decision support, renewable energy awareness, and financial incentive spreadsheet based tool. At the core of this tool, it standardizes multiple renewable energy designs, such that it may output the plausible energy generation, greenhouse gas reduction, and levelized cost of energy [26, 27, 29].

2.6.2 Sizing Tools

Based on the specified energy requirement of a PV system, a sizing tool will determine the most advantageous size of the various components. This could be constituted upon the size of the components that yield the most favorable energy generation, while other tools attempt to determine the size of the components that will yield the minimal levelized cost of energy. Sizing tools, such as HOMER, Hybrid Designer, and PVSYST, are often times compiled as software packages that have a user-friendly interface. Generally, system installers use these tools [26, 27].

2.6.2.1 Hybrid Optimization of Multiple Energy Resources (HOMER)

HOMER is a software program that is capable of modeling hybrid renewable microgrids for a range of energy sources. It was originally owned by NREL, but is now a private entity. HOMER's strength comes from its ability to perform multiple iterations for numerous system configurations and component sizes [26, 27, 30].

2.6.2.2 Hybrid Designer

Hybrid Designer is a free software program, developed by the Energy Research Centre at Cape Town University. This program utilizes a genetic algorithm to evaluate multiple system configurations

that provide acceptable reliability, in order to determine the system that has the optimal levelized cost of energy [26, 27, 31].

2.6.2.3 PVSYST

PVSYST is one of the most commonly used software programs for designing a PV system. This program is able to combine multiple BOS components with a pre-feasibility study, such that hourly simulations of a complete PV system are performed. In doing so, the user selects components from the built-in database, and the software calculates the size of each component. However, PVSYST cannot analyze multiple systems at one time in order to find the case that yields the optimal levelized cost of energy. Therefore, the user usually performs a sensitivity and risk of investment analysis [26, 27, 32].

2.6.3 Simulation Tools

Currently, copious amounts of software tools that can simulate a PV system are available. The tools all function in a similar pattern, where the user characterizes each component, various loads, location, etc. Following, the program will simulate the system and outputs the energy generation and expected consumption as a function of time. Some tools, such as Hybrid2, PVSYST, and PV-DesignPro-S also compute a financial analysis [24, 26, 27]. Table 2.2 is a summary of some of the simulation tools available.

Table 2.2. Simulation software tools available

Software Tool	Source
Ashling	Consortium formed by NMRC (Ireland), ARMINES (France), ICI (Romania), and IMIO (Poland)
Hybrid2	NREL (USA)
INSEL	University of Oldenburg (Germany)
PV-DesignPro-S	Maui Solar Energy Software Corporation (USA)
PVSYST	Geneva University (Switzerland)
RAPSIM	Murdoch University (Australia)
SAU/AREA	Cardiff University (United Kingdom)
SOMES	Utrecht University (Netherlands)
SOLSIM	IAF/EWIS (Germany)
WATSUN-PV	University of Waterloo (Canada)

2.6.4 Shortcomings of the Current Solar Photovoltaic Modeling Tools

Pre-feasibility tools such as RETScreen are advantageous because they have the ability to compare multiple renewable energy technologies. However, these programs usually do not have a current financial and product database, which may cause a dilemma when comparing two or more similar technologies. Sizing tools such as PVSYST are beneficial because of the considerable modeling capabilities. However, some of these programs require extensive knowledge about the BOS, and are not always intuitive, and in some cases, these tools are incapable of incorporating a hybrid PV system. While there are many simulation tools available that can accurately quantify the plausible energy generation, these tools do not have the ability to simulate and compare multiple PV system designs at one time. Furthermore, a program can couple sizing and simulation, such as the idea behind PVSYST, but also provides the layout is advantageous for engineers, dealers, etc [26, 27].

2.7 United States Solar Photovoltaic Market

The recent trends in the solar PV market are astonishing. Referring to Figure 2.15, the amount of installations in the United States increased from 4 MW in 2000 to almost 4.8 GW in 2013. This quick growth in installations has been driven by government policies favoring renewable energy and a sharp decline in costs. From 2012 to 2013, the capacity-weighted average installed costs decreased from $3.04/W to $2.59/W, which is a 15% decline. However, this market is extremely dynamic, meaning that the installed prices have a large variance from project-to-project and state-to-state. For instance, the 2013 common residential prices stretched from just under $3.00/W to just under $7.00/W, whereas non-residential prices range from $1.70/W to $8.00/W, and utility prices range from $1.68/W to just over $3.00/W [33].

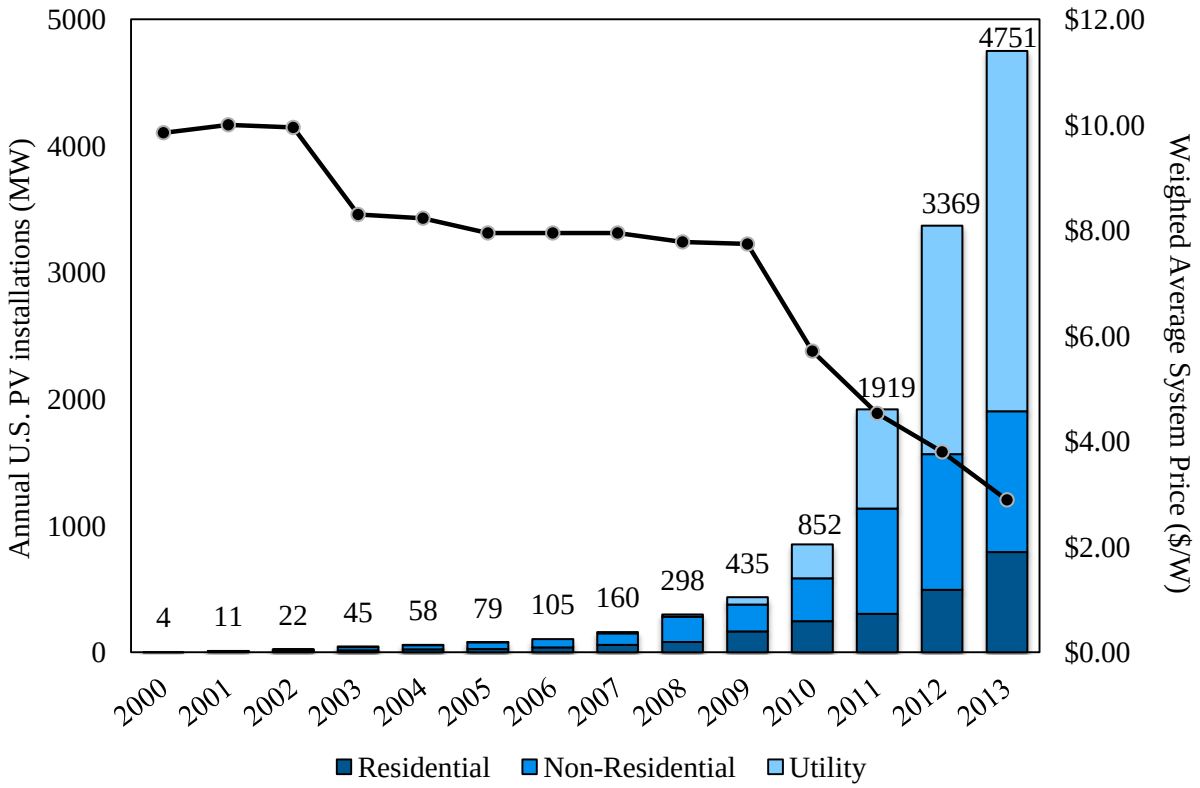

Figure 2.15. The 2000-2013 U.S. Solar PV installations and weighted average system price [33]

While the US PV market has been exponentially growing each year, the number of installations remains relatively concentrated in a few key states, as represented in Figure 2.16.

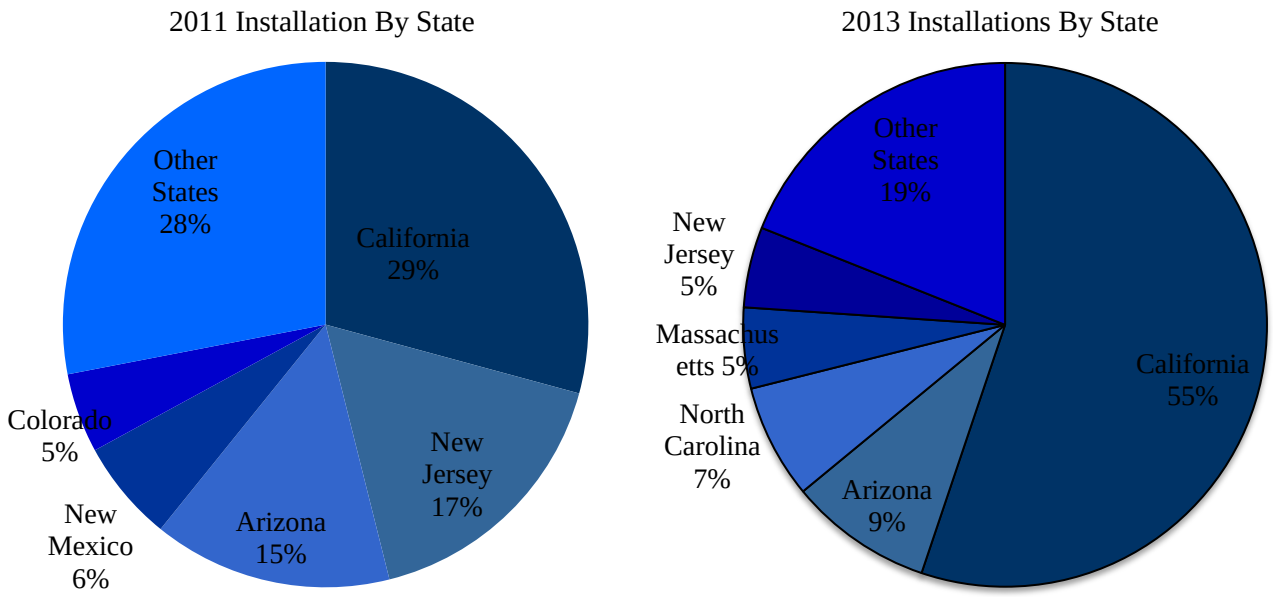

Figure 2.16. The 2011 and 2013 state-by-state solar PV installations by capacity [16, 33]

The solar PV industry consists of two markets, domestic and international, where the international market had a substantial influence on the reduced solar PV system costs. This began in 2007 when new restrictions pertaining to the production of raw silicon came into effect. By 2011, manufacturing worldwide increased by 100-fold, where China and Taiwan were responsible for producing 61% of the global PV module supply. However, this high level of production also contributed to numerous bankruptcies and consolidations, which eventually led to an investigation from the Department of Commerce. The investigation determined that the Chinese Government was subsidizing the cost of crystalline-silicon modules, meaning that PV modules were sold below production costs. This is known as 'illegal-dumping' and large tariffs were applied to Chinese modules as result [34].

2.7.1 Incentives and Initiatives

The federal, state, and local governments have grown increasingly aware of the economic, environment, and societal benefits of implementing renewable energy. As a result, many incentives and programs have been created such as the 2011 DOE SunShot Initiative. The DOE SunShot Initiative is a collaborative nationwide initiative that aims to reduce the total costs of solar electricity by 75% from 2010-2020, thus making solar energy competitive with traditional technology. The study outlining the initiative states that solar energy by 2030 may generate 14% of the US electricity needs and 27% by 2050. This would result in an 8% decrease or 181 million metric tons of CO_2 reduced by 2030, and 28% or 760 million metric tons by 2050. If the aforementioned scenario comes to fruition, 290,000 new solar jobs are projected to be created by 2030, and 390,000 by 2050. The SunShot Initiative price targets and reference targets are shown in Table 2.3, where these reference targets were calculated by Black & Veatch in 2012 [35].

Table 2.3. DOE SunShot Initiative benchmark and target prices

Market	Benchmark 2010 Price	Reference 2020 Price	SunShot 2020 Target Price
Utility Scale PV ($/$W_{DC}$)	4.00	2.51	1.00
Commercial Rooftop PV ($/$W_{DC}$)	5.00	3.36	1.25
Residential Rooftop PV ($/$W_{DC}$)	6.00	3.78	1.50

A common way to facilitate renewable energy projects is renewable energy credits. A renewable energy credit is much like purchasing clean electricity from the utility company, but this program is voluntary, meaning it allows a business to choose what projects to support, i.e. wind, solar, geothermal, etc. When renewable energy sources generate electricity, it is separated into two categories, electricity produced and environmental benefits. Based on what the user wants, the user either chooses electricity produced in MWh increments, or environmental attributes [36].

Another program is the Public Utility Regulatory Power Act of 1978 (PURPA), which requires the local utility company to purchase any excess renewable energy from a grid-tied system, at a rate equal to what it costs them to produce power. An additional program is third-party power purchasing agreements, which are designed to create incentives for the owner, consumer, and utility company. The DOE and the North Carolina Solar Center have created the Database of State Incentives for Renewables & Efficiency (DSIRE) in order to track the programs that help meet the needs of the owner, consumer, and utility company [37, 38].

2.7.2 Overview of the Bottom-Up Installed Price Benchmark

NREL and the US DOE published in February, 2012, the *Residential, Commercial, and Utility-Scale Photovoltaic (PV) System Prices in the United States: Current Drivers and Cost-Reduction Opportunities.* In this report, a range of solar PV costs using a bottom-up price analysis was assessed using Monte Carlo simulations. A Monte Carlo simulation is a statistical sampling method to approximate solutions to quantitative problems. More specifically, a Monte Carlo simulation transcribes uncertainties from the model inputs, by specifying the inputs as probability distributions, and creates model outputs based on the inputs [39].

As mentioned previously, there has been a significant decrease in the price of solar PV systems from either the global market players or governmental incentives. However, primarily due to the fair market value consideration on system prices, system cost reductions are not recognized, nor recognized in a timely manner. This is in large part due to the separation between installation costs, component prices, and system prices. Additionally, fair market value does not provide clear enough prices for understanding

the drivers in the system price. Therefore, this section describes overnight capital costs for commercial rooftop solar PV, developed from a bottom-up price analysis methodology [40].

For the analysis, NREL compiled a list of the estimated bill of materials (BoM) costs, which not only included material related costs, but also installation labor costs. In the report, it stated that the estimated direct labor costs were sensitive to changes in independent variables such as module and string size, module efficiency, and other system design parameters. Furthermore, the list subdivided some material categories such as wiring, where it included many components such as wire, conduit, and connectors, but excluded installation labor because it was in another category. Additionally regarding wiring materials, this category was broken down into two groups, DC and AC. A carpenter or general laborer may install the DC wiring components, which contains all the components from the module to the inverter, such as the combiner box and lighting rod, but excludes the inverter. A skilled electrician typically installs the AC wiring components, which includes all the components from the combiner box to the application, but excludes the utility substation if needed [40].

The pricing benchmark for rooftop commercial PV systems includes building types such as:

1. Architecturally unique buildings such as churches
2. Big-box offices
3. Office buildings more than two stories
4. Warehouse buildings one-two stories
5. Skyscrapers

Generally, a commercial rooftop has minimal to no slope and surface of asphalt, ballasted-membrane, or standing-seamed metal. The pricing benchmark for commercial rooftop PV systems includes: architecturally unique buildings such as churches, big-box offices, office buildings taller than two stories, skyscrapers, and warehouse buildings that are one to two stories. Furthermore, based on a building's preexisting features and region-specific system design requirements, a significant variance in the cost and design of the system arises. An example of a design variance based on a building's preexisting features is a roof that has a inverted roof membrane, which requires an anchored-ballasted

roof racking structure for the PV system. Region-specific system design requirements may include meeting municipal and county seismic standards. Alternatively, a region-specific system design requirement is the load capacity of the building. For example, areas in the U.S. where snow is eminent, buildings are already designed to be able to handle the load of a PV system; elsewhere areas that do not typically receive snow have a roof with a much more limited weight bearing capacity. In culmination, preexisting building features and region-specific system design requirements affect the design and hardware of the system, and how the system is installed, thus affecting the overall cost of the system [40].

In this report, it was stated that an experienced eight-person crew, using the direct-attach method for standing metal seam rooftops, can install up to 150 modules per day. In contrast, this experienced eight-person crew, using the method for flashed point penetration for through-roof systems, where approximately 0.07 penetrations per module are required, can install up to 25 modules per day. However, this experienced eight-person crew, using the through-roof rail-type system, can install up to 600 modules per day. Nevertheless, this experienced eight-person crew, depending on project staging techniques and local building requirements, using the ballasted mounting system, can install up to 1,000 modules per day. The ballasted system compared to the standing-seam mounting system, may provide 15-20% labor savings. However, the ballasted system is generally limited to membrane type roofs, and low to no roof slope [40].

The labor costs for the installation were calculated from the U.S. national average wage rates and standard burden rates. The national average for an electrical contractor before insurance and benefits is $49.00/hour, whereas the general contractor is roughly $33.00/hour. These averages took into account payroll taxes, retirement, health and liability insurance, and operating overhead costs that were varied by market sector, installer size and experience. The burden labor rates, included a 0.44% builders insurance, 6.2% federal and state unemployment insurance, 2.02% public liability insurance, 7.65% Social Security taxes (FICA), and 6.4% worker compensation insurance. It is projected that as more solar PV installations occur nationwide, large cost reductions in overhead and cost of trips for permits are to follow, as well as more efficient means of gaining permits. Collaborating installers have reported that the economy-of-scale

and standardized ground-mount systems leads to utility scale installations having the lowest project overhead costs per kW installed, followed by commercial rooftop installation, and then residential systems [40].

2.7.2.1 Bottom-Up Installed 2010 Benchmark Prices

The Monte Carlo Simulation for commercial solar PV rooftop analyzed a three-story building with a standing-seam system design. The simulation analyzed a system for 914 crystalline silicon modules that were 0.992 m by 1.653 m, and had an efficiency of 14.5%. They were installed on a standing-seam metal roof without through-roof penetration anchors, and were mounted using four clips per module. The overhead costs used in the system total $12,000, which was the culmination of building permits, commissioning and engineering expenses. The building permits, which included delays caused by permit-related activities, and commissioning costs such as utility upgrades to the building's electrical panel, totaled roughly $2,000, whereas the engineering was estimated at $10,000. However, some areas reported a permit fee as high as 10% of the project costs, which is not the case at Michigan State University [40].

The result of the Monte Carlo Simulation determined the 2010 price benchmark for commercial solar PV system rooftop of $4.59/W. Figure 2.17 details the 2010 element price benchmark breakdown, where modules are 45% of the total system price and is the largest contributor. The second and third largest contributors, 14% of the total system price, are the supply chain costs and installation materials, followed by the inverter being 8% of the total system price [40].

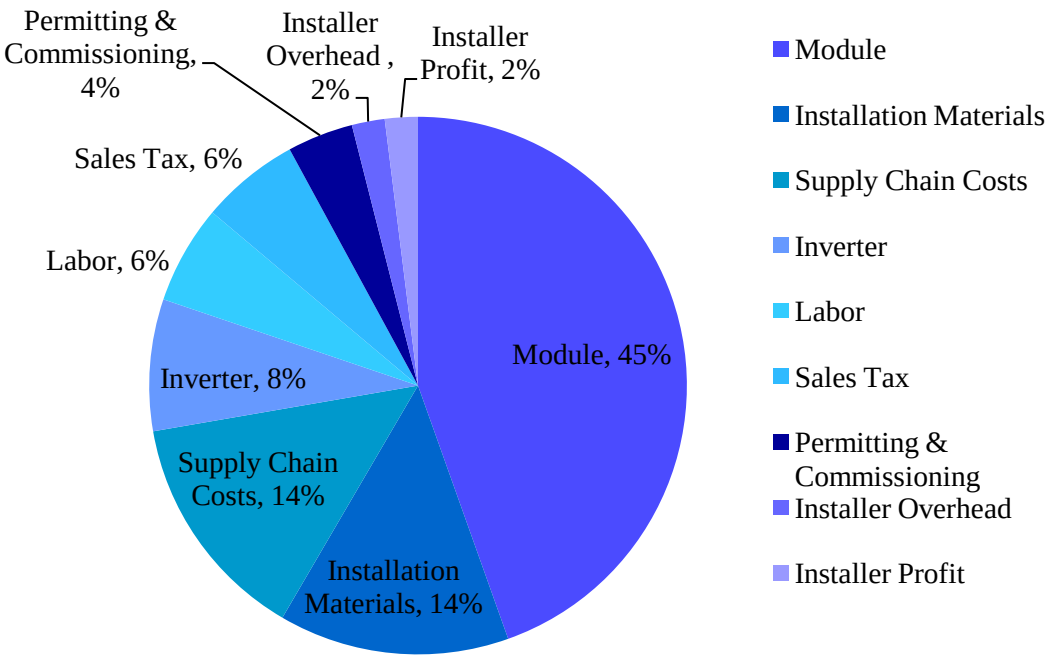

Figure 2.17. 2010 commercial rooftop PV system element breakdown [40]

Chapter 3 **FORMULATION OF THE PHOTOVOLTAIC SYSTEM COMPOSITION**

With the anticipated growth and dynamic complexity of the solar photovoltaic (PV) market, along with the large capital cost of PV systems, a need for a planning tool that will assist in the design of PV systems is desired. A wide variety of planning tools are currently available, as discussed in Section 2.6, for analyzing a PV system, where typically these tools are classified into three categories: pre-feasibility, sizing, and simulation. A prefeasibility tool determines if a specified application is financially feasible, while sizing tools establishes the size of the balance of system (BOS) components, and simulation tools provide a detailed analysis of the expected energy generation by emulating the PV system [24]. However, a robust planning tool does not exist that can take into account the complex geometry of a rooftop for multiple PV modules and tilt angles, while being able to analyze an assortment of component databases for the BOS, such that a multitude of solar PV system designs are created [24]. Therefore, this section of the thesis introduces a tool that takes a ubiquitous approach towards analyzing rooftop potential that can lead to ideal configuration designs and cost-effective building targets.

In reference to Figure 3.1, a procedure is characterized for relating global coordinates to the blueprint via image processing and pseudo-3D mapping. Then, a scheme for simulating the sun precession around the building is outlined and utilized to eliminate areas with a substantial degree of shading. A strategy for parametrically determining the layout of the modules and sizing the BOS, as well as simulation of plausible energy generation is developed. This design methodology is demonstrated on two case studies: the first case presents a comparison of an existing PV system to the planning tool, the second case study portrays the ability of the planning tool designing a PV system on a geometrically complex rooftop.

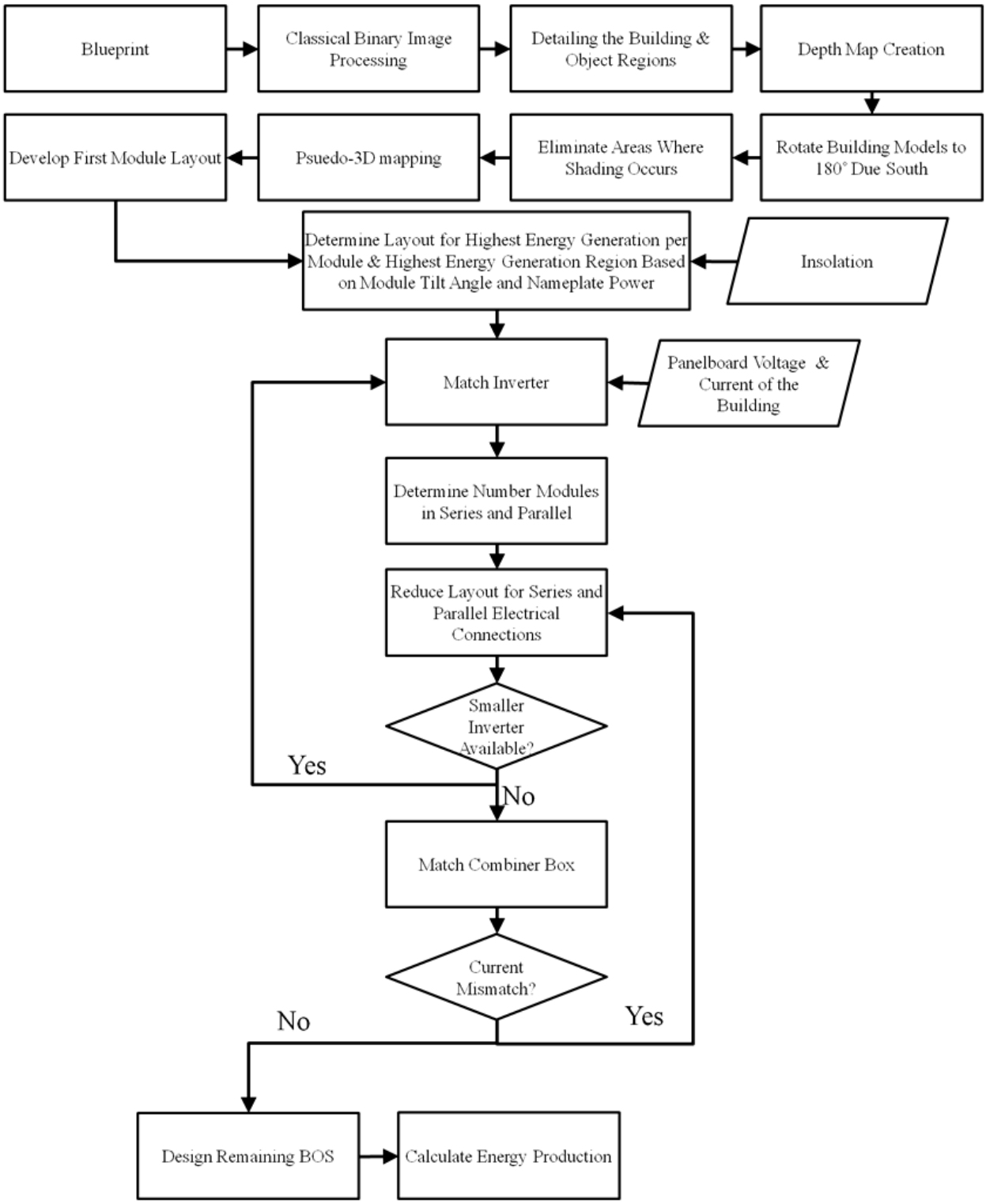

Figure 3.1. Flow chart illustrating the methodology employed for a solar PV system design that can be tailored to a building rooftop

The procedure for creating the virtual replica of the building begins with an image file format of the rooftop blueprint. Then binary image processing is employed to extract the various roof regions. This is followed by specifying the geographical location and orientation of the building, as well as details pertaining to the individual roof regions. Some of these details aid in the creation of the depth map, while other specifics develop the components needed for pseudo-3D mapping (see details below), a common technique in computer graphics that creates a virtual scaled model of the building. Pseudo-3D mapping was chosen because it is able to associate a scale with Cartesian coordinates. Next, the movement of the sun is simulated and the areas of the roof that experience a large amount of shading are eliminated. This is because the shaded modules act as load by consuming the power from other modules. This load consumption causes harmful excessive heat, which results in failure before the expected lifetime [14]. Following, an iterative procedure is performed for 2 output targets: 1) maximizing the amount of modules on a roof region for two module orientations and a multitude of tilt angles, and 2) creating optimized BOS designs based on the electrical specifications of the building. Finally, calculations are performed for simulating the expected energy generation for multiple PV system designs.

3.1 Image Processing of the Blueprint

The design of a PV system is streamlined by incorporating image processing of the blueprint. Previously this has not been done, but it has the following advantages: 1) evaluating an unlimited number PV system components; 2) assessing a multitude of module layouts and orientations; 3) providing a high degree of dimensional precision for layout of the modules; and 4) substantially reducing analysis time.

Many of the blueprints provided were PDF files corresponding to 11x17'' sheets. In order to perform the image processing using MATLAB, the blueprints were rasterized using ImageMagick, from PDF to PNG file format at 200 pixels per inch [41]. ImageMagick was used because it is a free software suite for displaying, converting, and editing files with Windows Software Development Kit [42]. The PNG file format was chosen because it supports lossless data compression [43].

3.1.1 Extracting the Roof Regions

A typical blueprint image is described as a 2D array of *n* rows by *m* columns of three-byte pixels that correspond to the primary colors red (*R*), green (*G*), and blue (*B*). However, to extract the roof regions from the blueprint, the blueprint must be an *n x m* binary file. This conversion is executed by initially removing any noise on the image using a Wiener filter, then, the image is converted from color to grayscale and finally into an *n* x *m* binary image of the blueprint [43].

The object regions of the binary image are extracted by implementing a connected component labeling operation. This process is described in [43, 44] and results in a connected component matrix that is the equivalent size of the binary image. Figure 3.2 depicts an exemplar connected components matrix containing sixty-three unique shades that represent the sixty-three unique object regions. Following, information about each object region is obtained such as the binary area and global pixel locations.

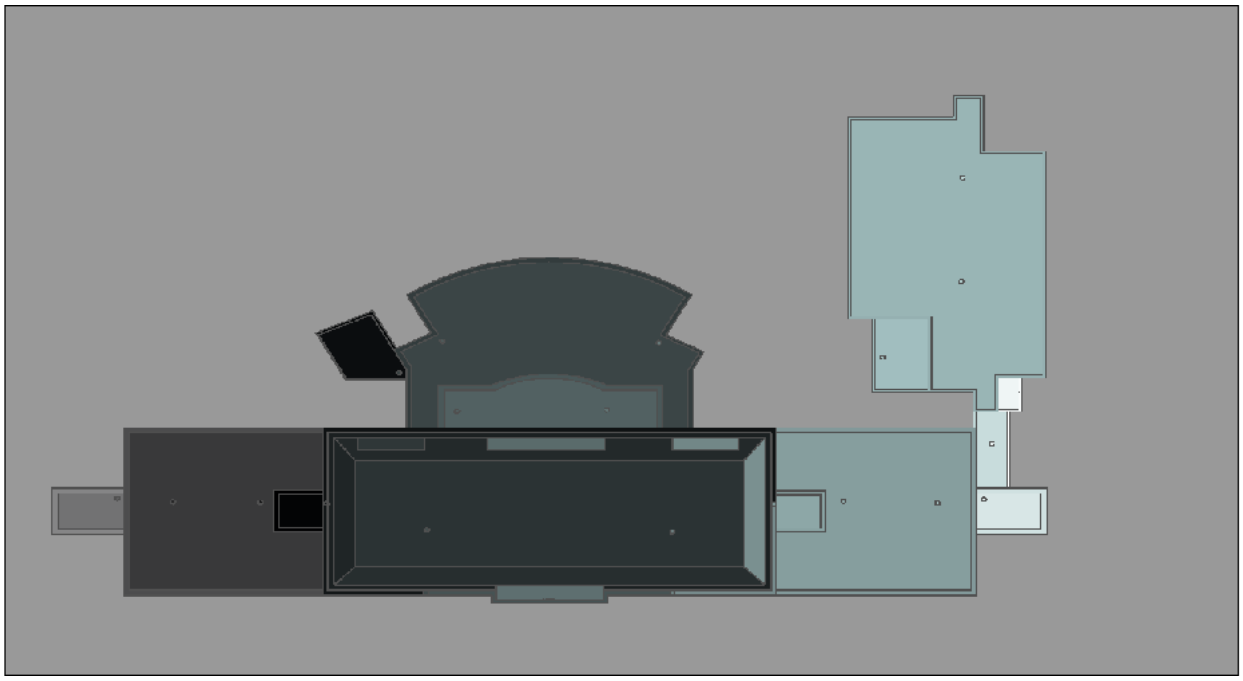

Figure 3.2. Image corresponding to connected components matrix, where each shade represents a different object region. There are sixty-three unique object regions depicted

After the image has been enhanced and subdivided into informational object regions, details are specified for each object region and the building as a whole. The entered data includes:

1. The size and scale of the blueprint
2. The longitude, latitude, and azimuth of the building
3. A label for each object region, including viable locations for the PV system (some regions may be deemed unviable due to buildings code restrictions)
4. The region pitch

3.1.2 Depth Map

The depth map of the building *DM*, referred to as the *z*-coordinate, is the same *n x m* dimensions as the blueprint. It is created by relating the pixel-by-pixel location of connected components matrix, to the corresponding height of the object region. If an object region has a pitch, the program relates the four selected corners by a series of vectors, such that four planes are constructed. Then the pixel-by-pixel location values of each plane are heuristically averaged together, eliminating outlier values, and related to the depth map. Outlier values may come into existence when the selected corner is not at the outer corner of the sloped region.

3.1.3 Roof Shade Modeling

The ensuing steps require rotating the binary, connected components, and depth map matrices, as well as the blueprint image files, such that the building is orientated with respect to its geographical coordinates. This not only aids in quantifying the location of the sun throughout the day, but also provides the setup for the layout of the modules.

The seasonal angles required to describe the location of the sun with respect to the design of the PV system are depicted in Figure 3.3, where Σ is the module tilt angle, δ is the declination angle, θ_a and θ_z are the solar altitude and zenith angles, respectively, and ϕ_c and ϕ_s are the sun and module collector face azimuth angles, respectively. The amount of shade that each region of the building experiences is calculated using the Winter Solstice Altitude Angle, α_W. At this sun angle, the effects due to partial shading on the modules are reduced. If a module experiences partial shading, an electrical resistance

within the module occurs, which result in harmful excess heat, such that failure is encountered before the expected lifetime of the module [14, 45].

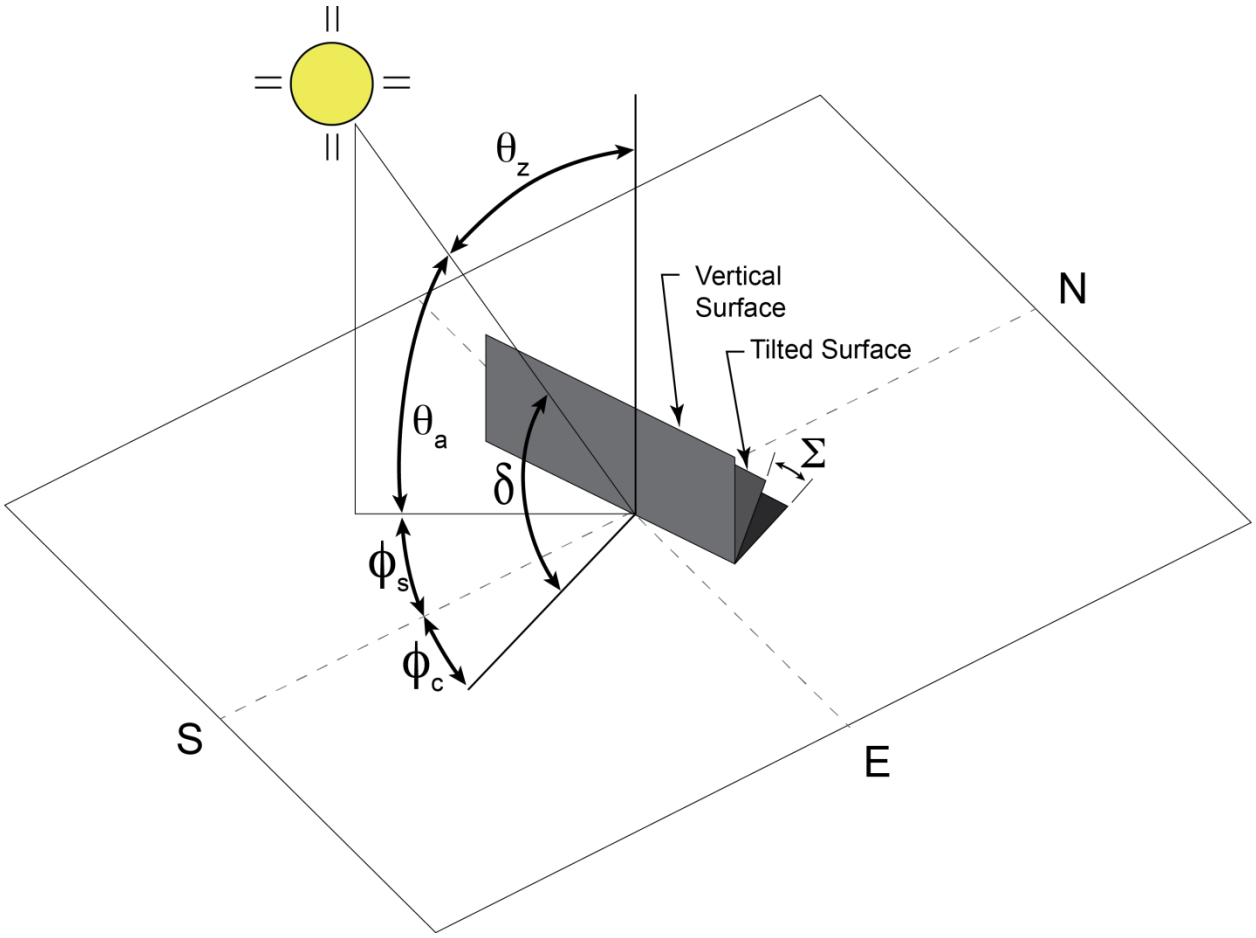

Figure 3.3. Various sun angles used to calculate the shade

The amount of shading that occurs on each object region can be determined in several ways, for instance, a ray-tracing algorithm. However, implementing a ray-tracing algorithm is computationally expensive, and surrounding objects such as neighboring buildings are not distinguished on the blueprints [46]. Instead, the amount of shade that the building rooftop experiences is determined using simple geometric concepts that are associated with the pixel-by-pixel values within the depth map. Subsequently, a matrix the same size as the depth map is generated, and locations that experience shade are flagged. The basic algorithm used is

$$\text{Shade}_{i\,j} = \frac{DM_{i\,j} - DM_{i\,j-1}}{\tan(\alpha_W)}, \text{ where } 1 \le i \le n \text{ and } 2 \le j \le m$$

Then, the shade matrix is superimposed with the connected components matrix, and areas containing shade are eliminated since the cost of maintenance and performance reduction in these regions outweigh the benefit of additional collection area.

3.1.4 Pseudo-3D Mapping

Although the *DM* of the building may be viewed as 3D model, it does not have a dimensional correlation to the physical environment. Thus, due to the module layout employing a systematic dimensional analysis scheme, discussed in Section 3.2, a scale must be associated with the *x*, *y*, and *DM* pixel coordinates. This may be achieved a number of ways, for instance, creating a point cloud and meshing each point with a series of triangles that may be thought of as planes. However, given the post-processing design of the module layout, incorporating pseudo-3D mapping, sometimes referred to as 2.5D point mapping is a better fit. The 2.5D point mapping strategy is commonly used in the development of human face models and video games, where each mapped point specifies a 2.5D projection of a surface, in this case a building, in 3D space [47, 48].

The 2.5D point mapping technique requires three matrices that correspond to the *x*, *y*, and *z* coordinates, a flag matrix, and the rotated color blueprint image. The flag matrix is required to account for missing information, and as stated previously, the *z* coordinate is the *DM*. The *x* and *y* matrices, commonly referred to as 2.5D column and row matrices, are *n x m* arrays the same size as the *DM*. Each column or row value in the *2*.5D matrices grow in a successive fashion to a specified value, in this case, the actual size of building [47]. The technique can be visualized as

$$\text{2.5D Projection Point}_{(i,\,j)} = \{Row_{(i,\,j)}, Column_{(i,\,j)}, DM_{(i,\,j)}, r_{(i,\,j)}, g_{(i,\,j)}, b_{(i,\,j)}, Flag_{(i,\,j)}\},$$
$$\text{where } 1 \leq i \leq n \text{ and } 1 \leq j \leq nm.$$

Figure 3.4 depicts the original RGB blueprint, *DM*, 2.5D row, and column matrices. The lighter shades of gray in 3.4c and 3.4d correspond to larger values of the row and column matrices, respectively. When the three matrices are superimposed with the RGB blueprint image, it culminates into a 2.5D projection that corresponds to the actual building.

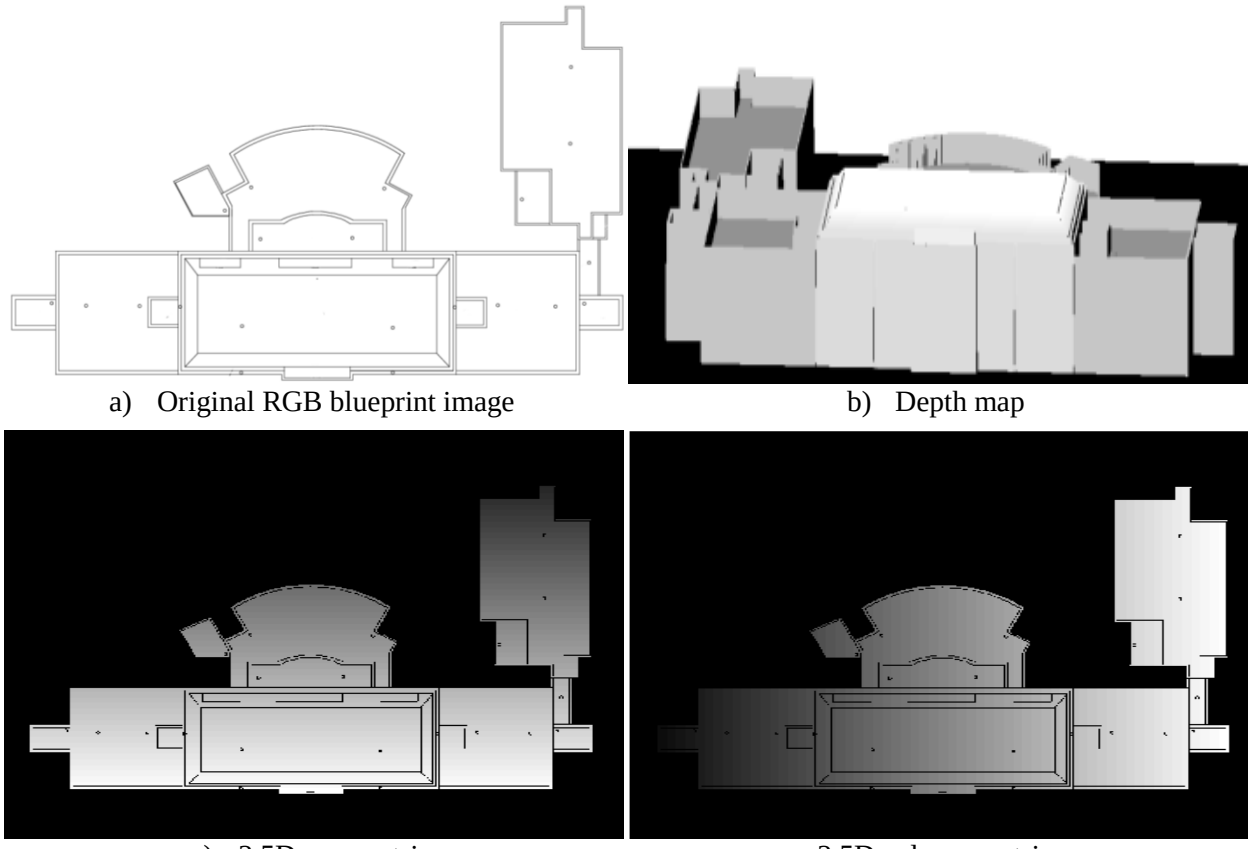

a) Original RGB blueprint image b) Depth map

c) 2.5D row matrix 2.5D column matrix

Figure 3.4. Images representing the matrices incorporated in 2.5D mapping. The lighter shades in c and d correspond to larger pixel-by-pixel values

Following this procedure, the object regions are separated into a set of binary *n x m* matrices for the module layout. For this thesis, the matrices referring to the binary object regions are also called the viable panel regions.

3.2 Layout of the Modules

The goal of the module layout procedure is to identify a layout that will maximize the number of modules in each region. While this is a well-studied concept there has been considerably less research conducted towards characterizing an algorithm that will maximize rectangular shaped objects in an irregular area [49, 50, 51]. Nonetheless there have been numerous studies aimed at identifying the most advantageous PV configuration pertaining to the electrical distribution, module tilt angle, sizing ratios of the PV modules to the inverter, and sizing for load applications [52, 53, 54, 55, 56]. However, these studies are not as applicable because these configurations require a uniform number of modules connected

in series, which may not be the case when rooftop is geometrically complex. Considering that the modules are maintained at a fixed tilt angle, and have the same characteristic properties such as dimensions and nameplate capacity, i.e. the PV system only contains identical modules, allows for the assumption that the total spacing between each string *TS* is of fixed length. Additionally, because the goal is to uniformly fit as many modules into a region as possible, results in an algorithm that can perform numerical approximation of definite integrals, that can be viewed as Left Riemann Sums. Referring to Figure 3.5, the bounding curves of integration may be viewed as the outer perimeter of each viable panel region.

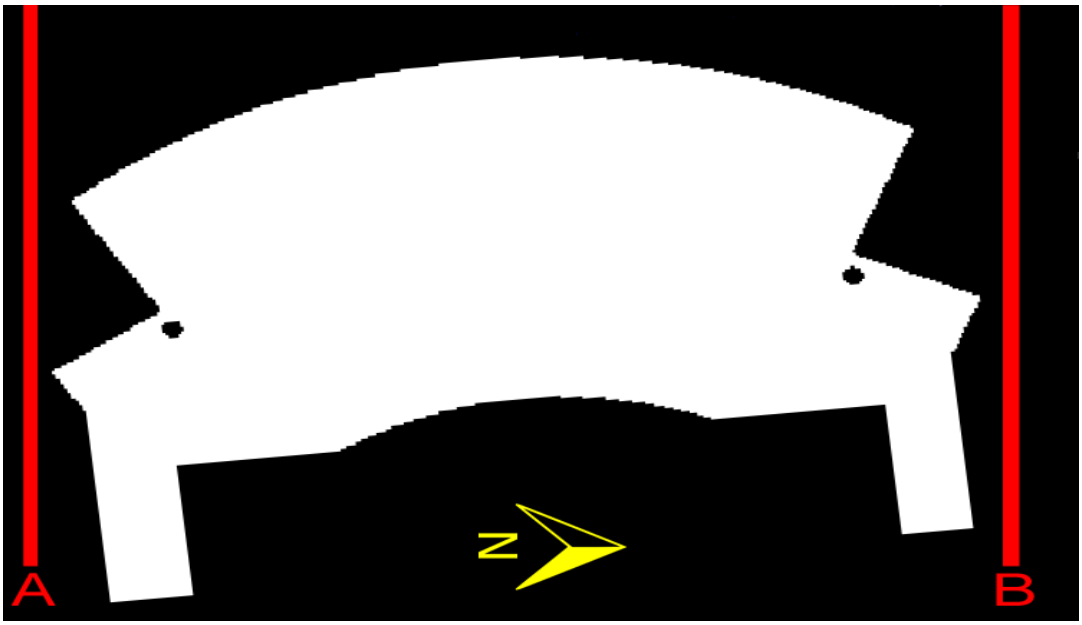

Figure 3.5. Representation of a viable panel region

Figure 3.6 describes the vectors used in the module layout, where *MP* is the module projection on to the ground and it is a function of module tilt angle and dimension L_2. The shade projection *SP* on to the ground due to the sun is calculated from the maximum module height above ground *H* and the high noon solar altitude angle α. These are

$$MP = L_2 \cdot cos(\Sigma) \tag{3}$$

$$H = L_2 \cdot sin(\Sigma) \tag{4}$$

$$SP = H \,/\, tan\,(\alpha) \tag{5}$$

$$TS = MP + SP \tag{6}$$

Thus, the total spacing *TS* between each string is the summation of the module projection and the shade projection.

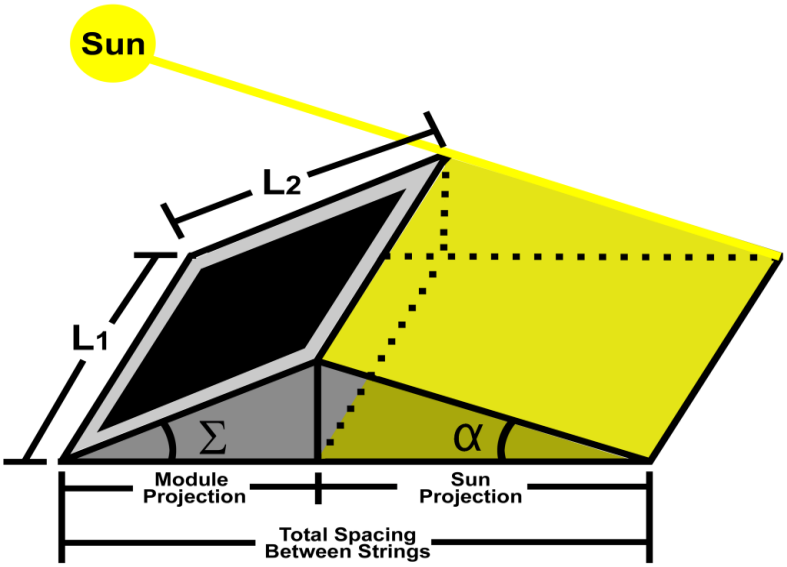

Figure 3.6. Description of the vectors employed in the layout of the modules

In reference to Figure 3.7, a string can be split into subintervals of modules connected in series. For example, each string in a PV system requires twelve modules; however, the layout of the modules has two subintervals *S*, that each contain six modules. These modules are connected in series via either module-to-module wires, or a pass through wire box.

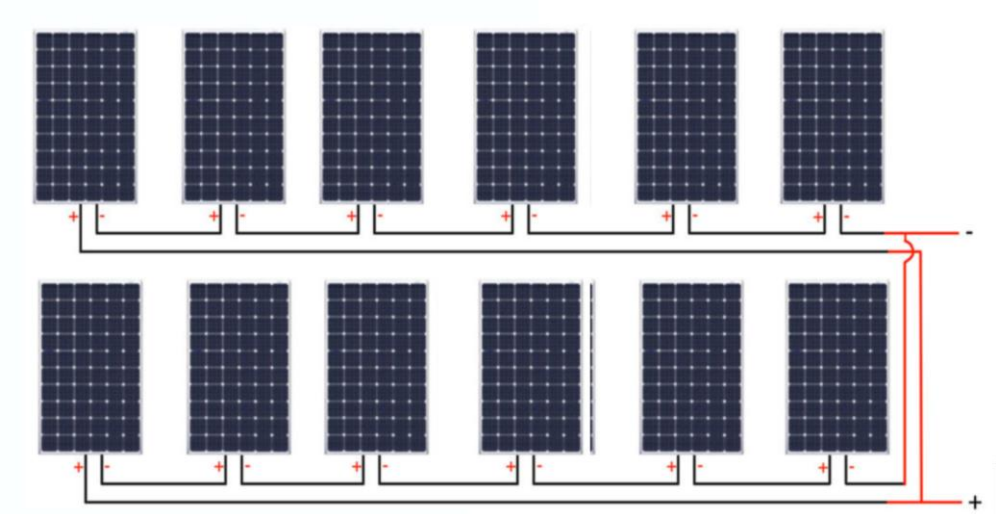

Figure 3.7. Illustration of how two string subintervals may be connected in series

The amount of string subintervals that can fit in the viable panel region is determined by

$$S = \ (B - A)/TS \tag{7}$$

where A and B are the minimum and maximum column values that correspond to the location of the viable panel region with respect to the 2.5D column matrix. The amount of subintervals is correlated to the column starting position on the binary matrix. Due to the binary matrix containing a length per pixel, there is a possibility that the shade from a subinterval could end in the same column as a string may start. In that case, a *flag* is stored that indicates that the column starting position of the binary matrix will be reexamined.

The algorithm for the layout of the modules references three main matrices: 1) binary, 2) 2.5D row, and 3) 2.5D column. The binary matrix determines where a module can be placed, and the 2.5D row and column matrices give the dimensions. The layout begins at the binary minimal row and column position for each viable panel region. Following, each binary row is summed along the column, the binary distance corresponding to the *MP*. If the sum of each binary row equals the binary projection, the 2.5D row and column values that coincide to the start and end position of that row are stored. When the last binary row of the subinterval is completed, the total distance that corresponds to the stored 2.5D row values is determined. Then this value is divided by the module length not used in the projection (in the case of Figure 3.6, this is the L_1 length), thus resulting in the amount modules that can fit in a subinterval. The aforementioned algorithm repeats for each subinterval start position. In addition, the last starting position of a subinterval plus the *MP* may not equal the last column of the viable panel region. Therefore, an iterative procedure where the binary start position for a subinterval is shifted until the last subinterval starting position plus the *MP* is equal to the last column of the viable panel region. Each iteration is then compared, and the iteration that supports the most modules is stored. Next, the orientation of the module is flipped, i.e. L_1 and L_2, and the code repeats. Lastly, each module orientation is compared, and the orientation that can support the most modules is stored for further processing. This algorithm was developed for a collection modules with a range tilt angles, and four solar altitude angles that correspond to the Winter and Summer Solstice and the Vernal and Autumnal Equinox at high noon.

3.3 Initial Energy Comparison & Inverter Characteristics

The maximum amount of modules that can fit in a region for the four altitude angles, multiple modules, and tilt angles ranging from 0-90˚ has been determined. Now the planning tool compares each module layout on the basis of power and energy. A derate factor *DF* may be applied without having to design the BOS. These *DFs*, presented in Table 3.1, account for the losses when converting from DC to AC at standard testing conditions (STC) [57].

Table 3.1. PV system component derate factors for DC to AC conversion at STC

Component Derate Factors	Range		
	Typical	Low	High
PV Module Nameplate DC Rating	0.95	0.8	1.05
Inverter and Transformer	0.92	0.88	0.98
Mismatch	0.98	0.97	0.995
Diodes and Connections	0.995	0.99	0.997
DC Wiring	0.98	0.97	0.99
AC Wiring	0.99	0.98	0.993
Soiling	0.95	0.30	0.995
System Availability	0.98	0.00	0.995
Overall Derate Factor	0.769	0.00	0.96

The expected AC power P_{AC} is a function of the system's DC rating and the inverter derate factor DF_{inv}. The DC rating is found by multiplying the maximum power of each module P_{mp} with the total amount of modules M in the system. The P_{AC} is determined by

$$P_{AC} = P_{mp} \cdot DF_{inv} \cdot M \tag{8}$$

Following, the base energy capability $G_{S\,t}$ of each layout is calculated. This is a function of the total quantity of modules in the system, the solar insolation entering the module's collector face $I_{c\,t}$ at a given time period, the area of the module A_{PV}, the efficiency of the module η_{PV}, and a system derate factor DF_{sys}.

$$G_{S\,t} = I_{C\,t} \cdot A_{PV} \cdot \eta_{PV} \cdot DF_{sys} \cdot M \tag{9}$$

The module efficiency is determined by the current and voltage at the maximum power point on the I-V curve, I_{mp} and V_{mp}, respectively, as well as the area of the module and the solar insolation at STC I_0 [8]. This is expressed as

$$\eta_{PV} = \frac{I_{mp} \cdot V_{mp}}{I_0 \cdot A_{PV}} \tag{10}$$

The layout that supports the highest energy generation per module and highest total energy generation is chosen for matching a preliminary inverter, where this inverter must have the same output phase ϕ and voltage V of the building [8].

3.4 Electrical Connections

Using Kirchhoff's Voltage Law in conjunction with the maximum operating voltage of the inverter $V_{inv\ mpp}$ and the module's open circuit voltage at STC $V_{oc\ 0}$, the number of modules in series M_S is found by

$$M_s = \text{floor}\left(V_{inv\ mpp}/V_{oc\ 0}\right) \tag{11}$$

As a result, the number of strings connected in parallel M_P is found by

$$M_p = \text{floor}(M/M_s) \tag{12}$$

The maximum operating voltage for the inverter is typically 70% of the maximum rated input DC voltage [58]. It should be noted that the *floor* function means to round down to the nearest whole number. In addition, the amount of strings is reduced if the short circuit current of the system is greater than the input current of the inverter.

After the number of modules in series and parallel has been determined, the layout of modules from the preliminary design is modified to match the electrical connections. The layout modifications are as follows: 1) if a region cannot support a string, it is eliminated; or 2) if a region of *x* number of strings has *y* modules remaining, the *y* remaining modules are eliminated as well. Due to the potential that modules from the regions are reduced, the inverter is reexamined for the possibility that a smaller inverter is available. If a smaller inverter is available, Eqs. (8) - (10), and (12) are repeated.

3.5 Sizing of the Balance of Systems

The BOS formulation being described is in reference to Figure 2.14 Figure 3.1. The wires from the strings transition via a pass through wire box into regular building wire typically referred to as

conduit. The input fuse rating for the box PTB_{FR} is a function of the short circuit current from a module $I_{sc\,0}$, the amount of strings that are entering the pass through box PTB_N, and a safety factor of 125% to be in accordance with NEC [8, 18, 24, 59], i.e.

$$PTB_{FR} > PTB_N \cdot I_{sc\,0} \cdot 1.25 \tag{13}$$

In the case of smaller systems, i.e. systems smaller than 1kW, the pass through wire box can be used as the combiner box. Consequently, in the case of larger systems, the conduit from the pass through wire box is fed into a combiner box [8, 18, 24]. The NEC handbook contains tables that determine the size of the conduit wire based on the amperage and type of conduit, where the type depends on its location within the system.

The input fuse rating of the combiner box C_{FR} is a function of the short circuit current of the module, the amount of strings entering/exiting the pass through wire box, a factor of 125% to account for higher insolation at lower temperatures and another factor of 125% for safe over sizing in accordance with NEC. The maximum input voltage rating of the combiner box C_{VR} is determined from the total open circuit voltage of the PV arrays, and a temperature correction factor from Table 690.7 of the NEC handbook [8, 18, 24, 59], i.e.

$$C_{FR} > I_{sc\,0} \cdot 1.25 \cdot 1.25 \tag{14}$$

$$C_{VR} > V_{OC} \cdot M_s \cdot (\text{NEC Correction Factor}) \tag{15}$$

The maximum output voltage of the combiner box is equal to the maximum input voltage. The maximum busbar rating, established during UL 1741 testing, defines the maximum continuous output current of the combiner box. The combiner box's maximum output current C_{Im} is determined by the number of inputs C_N and the open circuit current [8, 18, 24, 59], as

$$C_{Im} = C_N \cdot I_{sc\,0} \tag{16}$$

Due to the intricacy of the NEC codes, along with the dynamic complexity of the solar PV market, calculations for ground fault protection devices are not included. Furthermore, many inverters on today's market include ground fault protection devices and in some cases, DC array disconnects. However, in the case that the DC array disconnect is not included with the inverter, the disconnect input

fuse rating S_{IDC} must be sized in accordance with NEC 690. This is determined by multiplying Eq. (14) with the amount of strings connected in parallel, and dividing by the number of combiner box outputs C_o [8, 18, 24, 59].

$$S_{IDC} > C_{FR} \cdot M_P / C_o \tag{17}$$

To determine the size of the disconnect under normal operating conditions, a temperature correction factor F is applied as

$$F = \sqrt{\frac{T_{max,normal} + \Delta T_{max} - T_{amb}}{\Delta T_{max}}} \tag{18}$$

where $T_{max,\ normal}$ is the maximum allowed temperature during normal operating conditions, and ΔT_{max} is maximum allowed temperature rise specified by the manufacturer. These values are typically 40˚C and 85˚C respectively. Therefore the disconnect rating under normal conditions is then

$$S_{IDC\ MP} > I_{MP} \cdot M_P / (F \cdot C_o). \tag{19}$$

Additionally, the maximum input voltage for the disconnect may be sized using Eq. (15) [8, 18, 24, 59].

The inverter is initially selected using Eq. (8). Then, based on the manufacturer's specifications, the voltage of the PV system must be in agreement with the inverter [8, 18, 24, 59], i.e.

$$\text{Inverter Voltage Max} > V_{oc\,0} \cdot M_s \tag{20}$$

$$\text{Inverter Voltage Min} < V_{mp} \cdot M_s \tag{21}$$

These calculations assume that the number of DC outputs from the combiner box, do not exceed the number of inputs for the inverter. If so, the PV system will need more combiner boxes. The AC disconnect, according to the NEC, must be sized based on the outputs of the inverter. Equations (13) to (21) are for PV systems 600V DC or less; larger systems require special attention to NEC 690 [8, 18, 24, 59].

3.6 Simulation of the Energy Generation Capabilities

Two models are described in this section for determining the expected energy generation of a PV system. In the models, a module degradation factor *MDF* is included to account for the module

deteriorating over time, which is typically 0.5% each year [13]. The common calculation used in both models for determining the expected energy generation PV system in a given time period $G_{S\,t}$ is

$$G_{S\,t} = I_{C\,t} \cdot A_{PV} \cdot M \cdot \eta_{PV} \cdot DF \cdot (1 - MDF)^t \tag{22}$$

The simple model for calculating the expected energy generation of the PV system can be determined by applying Eqs. (10) and (22), along with solar resource data and information supplied on the module specification sheet [8].

The more complex model for determining the expected energy generation, and the one utilized here, is the SNL Photovoltaic Array Performance Model [60]. This model includes the electrical, thermal, and optical properties and is designed to be used in conjunction with hourly solar resource and meteorological data. An interesting attribute of this model is that it is applicable for an array, string, single module, or single solar cell. The temperature on the back-surface of a module T_m and the cell T_{cell} are given by

$$T_m = I_{C\,t} \cdot \left(e^{a+b \cdot WS}\right) + T_{amb} \tag{23}$$

$$T_{Cell} = T_m + \frac{I_{C\,t}}{I_0} \cdot \Delta T \tag{24}$$

The temperature on the back-surface of a module T_m, is a function of the insolation that enters the module collector face, the wind speed WS at 10 meters above ground level, and the ambient temperature T_{amb}. Additionally, two temperature coefficients *a* and *b*, couple the affects of wind speed and insolation on the temperature of the module. The solar cell temperature T_{cell} is a function of the module's back-surface temperature, the temperature difference between the solar cell and module back surface ΔT, as well as a ratio of the insolation entering the module collector face and the insolation at STC. The current and voltage derived from the SNL model are as follows

$$I_{sc} = I_{sc\,0} \cdot \left\{ I_{C\,t} \cdot \left[1 + \frac{dI_{sc}}{dT} \cdot (T_{Cell} - T_0) \right] \right\} \tag{25}$$

$$I_{mp} = I_{mp\,0} \cdot \left[1 + \frac{dI_{mp}}{dT} \cdot (T_{Cell} - T_0) \right] \cdot \left[C_0 \cdot I_{C\,t} + C_1 \cdot {I_{C\,t}}^2 \right] \tag{26}$$

$$V_{oc} = V_{oc\,0} + M_s \cdot \left[N_s * \delta(T_{Cell}) \cdot ln(I_{C\,t}) + \beta_{V_{oc}}(I_{C\,t}) \cdot (T_{Cell} - T_0) \right] \tag{27}$$

$$V_{mp} = V_{mp\,0} + M_s \cdot \begin{Bmatrix} C_2 \cdot N_s \cdot \delta(T_{Cell}) \cdot ln(I_{C\,t}) + C_3 \cdot N_s \cdot [\delta(T_{Cell}) \cdot ln(I_{C\,t})]^2 \\ +\beta_{V_{mp}}(I_{C\,t}) \cdot (T_{Cell} - T_0) \end{Bmatrix} \quad (28)$$

The terms C_0 and C_1 relate the current at the maximum power point to the effective insolation, whereas C_2 and C_3 relate the voltage at the maximum power point to the effective insolation. The number of modules and solar cells electrically connected in series is M_s and N_s respectively, and $\delta(T_{Cell})$ is the thermal voltage per cell at the cell temperature. Additionally, n is the diode factor, and $\beta_{V_{oc}}(I_{C\,t})$ and $\beta_{V_{mp}}(I_{C\,t})$ are temperature coefficients that relate the module's open circuit and maximum power point voltage as a function of the effective insolation.

3.7 Case Studies

The solar PV design tool is tested and verified on two case studies. The first case study corroborates the solar PV design tool by comparing it to an existing rooftop solar PV system at the Michigan State University Surplus Store. This case study is divided into two parts. The first part provides a comparison of the module layout and energy generation, based on the existing 44˚ module tilt angle. In the second part of this case study, the solar PV design tool will exhibit two designs for the layout of the module: 1) the highest energy generation per module on a yearly basis and 2) the highest energy generation per region on a yearly basis. The energy generation for each scenario is a function of the solar insolation, module tilt angle and the module efficiency. These scenarios are different because typically when the modules have a lower tilt angle, more modules can be placed into an object region as opposed to a higher tilt angle. Thus, the object region that contains more modules may produce more energy, but at a potentially higher cost/area. The second case study demonstrates the solar PV design tool's ability to develop a PV system when the viable panel regions are irregularly shaped. The module selected for the design is presented in Table 3.2 and has the same characteristics as the modules on the MSU Surplus Store.

Table 3.2. Installed module characteristics under standard testing conditions

Maximum Power	P_{mp}	210 W
Open Circuit Voltage	V_{oc}	33.6 V
Maximum Power Point Voltage	V_{mp}	26.4 V
Short Circuit Current	I_{sc}	8.33 A
Maximum Power Point Current	I_{mp}	7.95 A
Length	L_1	1,482 mm
Length	L_2	992 mm

3.7.1 Case Ia: Validation of the Solar PV System Design Tool

The Surplus Store on the campus of MSU is located at 42.43˚N, 84.50˚W, and has 90˚ azimuth. The yearly average energy demand is 470 MWh, an average base power load of 170 kW and peak load of 250 kW. The roof of this building is shown in Figure 3.8a, where the green highlighted area represents a 902m^2 area depicting the location of the PV system. The existing 40.3 kW PV system is comprised of 16 strings with 12 modules per string, which culminates into 192 modules tilted at 44˚. There are also 16-pass through wire boxes and one 16-input combiner box. Additionally, the system contains a 50 kW 3ϕ 480/277V inverter, a DC disconnect rated at 600V and 200A, and an AC disconnect rated at 480V$_{AC}$ and 72A. Figure 3.8b depicts the monthly average energy consumed by the building, as well as the amount of energy the PV system generates. According to this figure, the PV system generates roughly 10% of the building load. In this case study, the layout of modules from the PV design tool allowed for a four-foot perimeter around the edge of the roof.

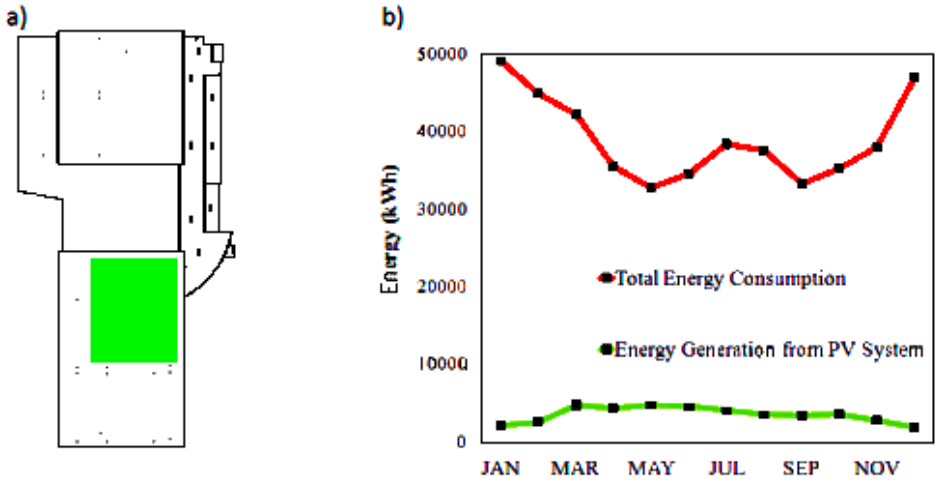

Figure 3.8. Michigan State University Surplus Store characteristics. The current PV System is located on green highlighted roof section in 3.8a. The average monthly energy demand is in section 3.8b.

When comparing the PV system at the Surplus Store to the PV design tool, the solar PV design tool recommends that 214 modules tilted at 44˚ (orientated such that L_1 creates the projection on the ground) can be fit in the space. Based on the number of modules and the building requirements, the tool determined that a preliminary inverter should be 3ϕ 480/277V and 44 kW or more. Then using the iteration described in Figure 3.1, the layout was reduced to 204 modules, comprised of 17 strings with 12 modules per string. Accordingly, the inverter for the system still had to be 3ϕ 480/277V but now has a minimal power rating of roughly 41 kW. Consequently, the program determined that 17 pass-through boxes were needed, and a combiner box that has 17 inputs with a DC disconnect requiring a minimum amp rating of 157A and 600V. The PV design tool established that the AC disconnect should be rated at 72A, which was based on the inverter's maximum over current protection per phase while at 480V. The results of this comparison are presented in Table 3.3.

Table 3.3. Design comparison of an existing solar PV system at the MSU Surplus Store vs. the solar PV design tool

PV System Attributes	Existing Solar PV System located on MSU Surplus Store			Potential Solar PV System located on MSU Surplus Store		
Module Layout	192 Modules	16 Strings	12 Modules Per String	204 Modules	17 Strings	12 Modules Per String
Amount of Pass Through Wire Boxes	16			17		
Combiner Box Characteristics	1 Combiner Box		16 Inputs	1 Combiner Box		17 Inputs
Inverter Characteristics	50 kW	3ϕ	480/277 V	41 kW	3ϕ	480/277 V
DC Disconnect Characteristics	600 V		200 A	600 V		157 A
AC Disconnect Characteristics	480 V		72 A	480 V		72 A

The results of the solar tool match relatively well, as far as the module layout and the sizing multiple components. Nonetheless, the calculation of the expected energy generation should also be accurate. The initial calculation determined that over the lifetime of the system roughly 225 kWh a year per module could be produced. Therefore, the energy derivation provided by SNL showed that over the lifetime of the system, approximately 216 kWh/year-module could be produced. The current system at the

Surplus Store produces about 219 kWh/year- module. Figure 3.9. illustrates a monthly comparison of the existing PV system versus the PV planning tool.

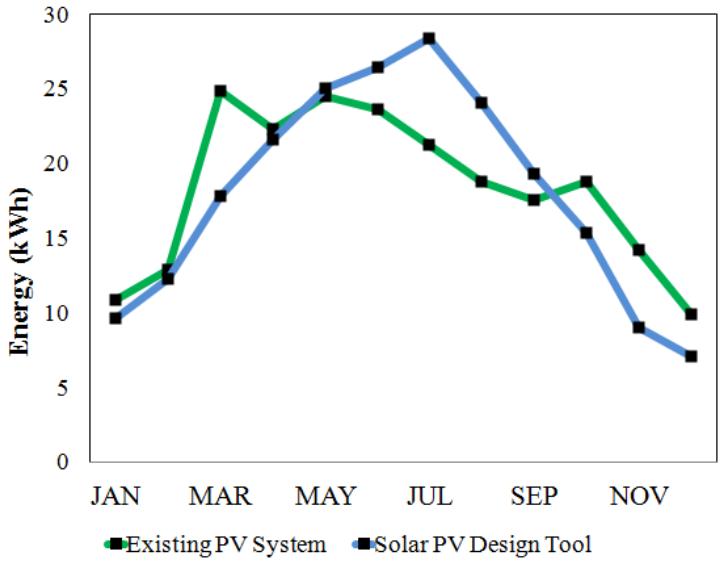

Figure 3.9. Monthly breakdown of the existing PV system compared to the solar PV planning tool

3.7.2 Case Ib: Energy Capabilities of the Solar PV System Design Tool

Continuing with the case study of the MSU Surplus Store, the solar PV design tool will exhibit two designs for: 1) the highest energy generation per module on a yearly basis and 2) the design for the highest energy generation per region on a yearly basis.

The situation resulting in the highest energy generation per module yielded that 243 modules tilted at 33˚ orientated such that L_1 created the projection on to the ground could fit in the space. As a result, based on the number of modules and the building requirements, the PV design tool determined that a preliminary inverter should be 3ϕ 480/277V and 49 kW or more. Following the iteration described in Figure 3.1, the layout was reduced to 240 modules, comprised of 20 strings with 12 modules per string. Accordingly, the inverter for the system still had to be 3ϕ 480/277V, but now a minimal power rating of roughly 48 kW is required. Then, the program computed that 20 pass through boxes were needed and a combiner box that was either 20 inputs or two combiner boxes that were each 10 inputs. Subsequently, the DC disconnect required a minimum rating of either 185 or 93A respectively and 600V. A 72A AC

disconnect was established by the PV design tool, which was based on the inverter's maximum over current protection per phase while at 480V.

The situation that yielded the highest energy generation per region determined that 603 modules, tilted at 0˚, orientated such that L_1 creates the projection on to the ground could fit in the space. Accordingly, the inverter for the system still had to be 3ϕ 480/277V but has a minimal power rating of approximately 121 kW. Using the same iteration scheme, the layout was reduced to 600 modules comprised of 50 strings with 12 modules per string. As a result, the inverter for the system was 3ϕ 480/277V with a minimal power rating of 120 kW. The program determined that 50 pass through boxes were needed and a combiner box that was either 50 inputs or two combiner boxes that were each 25 inputs. Subsequently, the DC disconnect required a minimum rating of either 462 or 231A respectively and 600V. A 72A AC disconnect was established by the PV design tool, which was based on the inverter's maximum over current protection per phase while at 480V. The results for both cases are summarized in Table 3.4.

Table 3.4. Comparison at the MSU Surplus Store of the solar PV system design for highest energy generation per module and highest energy generation per region

PV System Attributes	Highest Energy Generation per Module			Highest Energy Generation per Region		
Module Layout	240 Modules	20 Strings	12 Modules Per String	600 Modules	50 Strings	12 Modules Per String
Tilt Angle	33˚			0˚		
Amount of Pass Through Wire Boxes	20			50		
Combiner Box Characteristics	1 Combiner Box		20 Inputs	1 Combiner Box		50 Inputs
	2 Combiner Boxes		10 Inputs	2 Combiner Boxes		25 Inputs
Inverter Characteristics	48 kW	3ϕ	480/277 V	120 kW	3ϕ	480/277 V
DC Disconnect Characteristics	600 V		185 A	600 V		462 A
	600 V		93 A	600 V		231 A
AC Disconnect Characteristics	480 V		72 A	480 V		72 A

3.7.3 Case II: Complex Roof Geometries of the Solar PV System Design Tool

The second case study portrays the ability of the solar PV design tool to account for a geometrically complex rooftop and perform an economic evaluation. An exemplar rooftop on the campus

of MSU is the Psychology Building. This building is located on the North-Side of campus, at 42.73˚N, 84.55˚W, and has a 174˚ azimuth. The yearly average energy demand, shown in Figure 3.10b, is 1,300 MWh. The normal base load is 150 kW with a Summer peak load of 300 kW. Furthermore, the panelboard for this building is 3ϕ 480/277 V. Figure 3.10a depicts the roof of the Psychology Building, where the numbers 1-7 indicate the regions deemed viable for the installation of a solar PV system. Table 3.5 portrays the area of each region before and after the effects of shade.

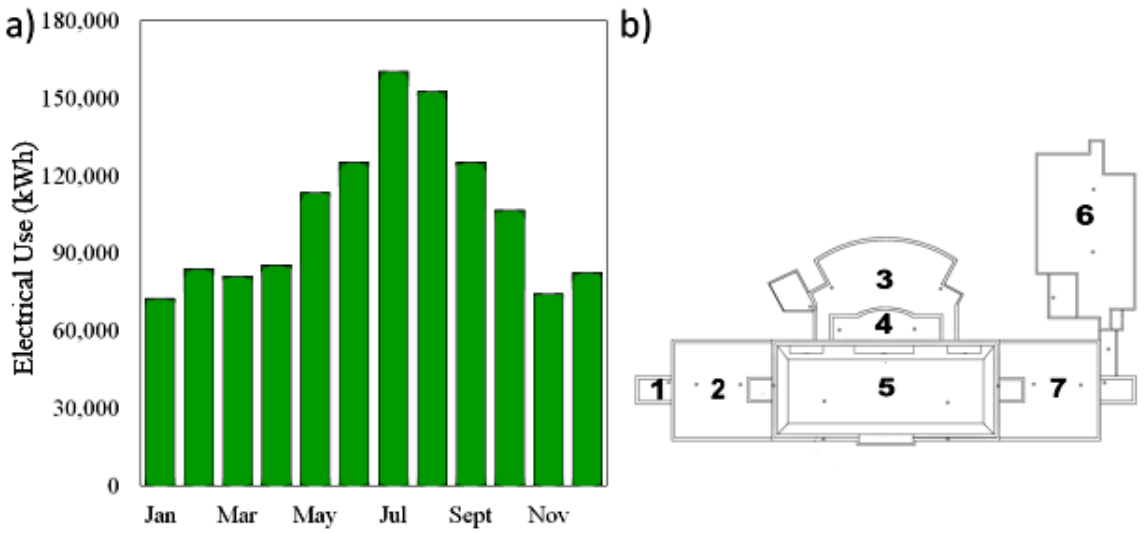

Figure 3.10. Characteristics of the Michigan State University Psychology Building. The labels 1-7 in 3.10a correspond to the regions employed in the layout of the modules. The average monthly energy consumption from 2007-2013 is shown in 3.10b.

Table 3.5. Total area of each region and area of each region after shade is included

Region	Area (m^2)	Viable Area(m^2)
1	26.7	16.1
2	339.9	291.0
3	365.9	320.4
4	103.1	93.4
5	489.7	489.7
6	524.3	431.1
7	341.3	239.3

The solar PV design tool will exhibit two designs for the layout of the module: 1) the highest energy generation per module on a yearly basis and 2) the highest energy generation per region on a yearly basis. The situation resulting in the highest energy generation per module yielded that 428 modules tilted at 33˚ orientated such that L_1 and L_2 created the projection on to the ground could fit in the space.

As a result, based on the amount modules and the building requirements, the PV design tool determined that a preliminary inverter should be 3ϕ 480/277V and 86 kW or more. Again, following the iteration described in Figure 3.1, the layout was reduced to 384 modules, comprised of 32 strings with 12 modules per string.

Accordingly, the inverter for the system still had to be 3ϕ 480/277V but now a minimal power rating of roughly 77 kW is required. The program determined that 32 pass through boxes were needed and a combiner box that was either 32 inputs or two combiner boxes that were each 16 inputs. Subsequently, the DC disconnect required a minimum rating of either 296 or 148A respectively and 600V. A 72A AC disconnect was established by the PV design tool, which was based on the inverter's maximum over current protection per phase while at 480V.

The strategy that yielded the highest energy generation per region determined that 1069 modules, tilted at 0˚, orientated such that L_1 and L_2 created the projection on to the ground, could fit in the space. The PV design tool determined that a preliminary inverter should be 3ϕ 480/277V and 214 kW or more. Again, following the iteration described in Figure 3.1, the layout was reduced to 1020 modules comprised of 85 strings with 12 modules per string.

Correspondingly, the inverter for the system still had to be 3ϕ 480/277V but now has a minimal power rating of approximately 204 kW. The program determined that 85 pass through boxes were needed. Given the combiner box product data base used in the program, a combiner box that could accept 85 inputs did not exist. In order to avoid current mismatch, the module layout was again reduced such that it now contains 1008 modules comprised of 84 strings with 12 modules per string. Thus, the inverter power rating was reduced to 202 kW, and the PV design tool determined that 84 pass through wire boxes were needed. As a result, the program determined that two combiner boxes of each 42 inputs, or three combiner boxes of 28 inputs. Assuming each combiner box had one output, the DC disconnect required a minimum rating of either 388 or 259A respectively and 600V. A 72A AC disconnect was established by the PV design tool, which was based on the inverter's maximum over current protection per phase while at 480V.

Table 3.6 displays the results of the module layout for both scenarios, while Table 3.7 presents the system characteristics for each design.

Table 3.6. The layout of the modules on the roof the MSU Psychology Building, for the highest energy generation per module on a yearly basis, and highest energy generation per region on a yearly basis

Region	Highest Energy Generation Per Module			Highest Energy Generation Per Region		
	Module Orientation	First Pass Modules	Second Pass Modules	Module Orientation	First Pass Modules	Second Pass Modules
1	L_1 or L_2	3	0	L_2	7	0
2	L_1	68	60	L_1	170	168
3	L_2	70	60	L_1	172	168
4	L_1 or L_2	19	12	L_1	46	24
5	L_1	111	108	L_1	287	276
6	L_1	102	96	L_1	250	240
7	L_1	55	48	L_1	137	132

Table 3.7. Comparison at the MSU Psychology Building of the solar PV system design for highest energy generation per module and highest energy generation per region

PV System Attributes	Highest Energy Generation per Module			Highest Energy Generation per Region		
Module Layout	384 Modules	32 Strings	12 Modules Per String	1008 Modules	84 Strings	12 Modules Per String
Tilt Angle	33˚			0˚		
Amount of Pass Through Wire Boxes	32			84		
Combiner Box Characteristics	1 Combiner Box		32 Inputs	2 Combiner Box		42 Inputs
	2 Combiner Boxes		16 Inputs	3 Combiner Boxes		28 Inputs
Inverter Characteristics	77 kW	3ϕ	480/277 V	202 kW	3ϕ	480/277 V
DC Disconnect Characteristics	600 V		296 A	600 V		388 A
	600 V		148 A	600 V		259 A
AC Disconnect Characteristics	480 V		72 A	480 V		72 A

The economic evaluation for the two situations is a culmination of the NREL 2010 bottom-up installed price benchmarks, discussed in Section 2.7, and the 4th quarter 2013 US Solar Market Insight cost variance, which is \$1.70/W to \$8.00/W with an average of \$3.57/W for non-residential installations [33]. In this analysis, the energy generated *G* from the PV system is considered the energy cost savings, where the commodity rate of electricity *CRE* is calculated as a flat rate, but is adjusted using the national

escalation rate of electricity *EE*, and is discounted with the prime lending rate *PLR*. The present value cost savings on a monthly scale is determined by

$$\begin{matrix}\text{Present Value}\\ \text{Energy Cost Savings}\end{matrix} = CRE \cdot G \cdot \sum_{t=1}^{T} \left(\frac{\left(1 + \frac{EE_{adj}^{(12)}}{12}\right) \cdot \left(1 + \frac{MDF_{adj}^{(12)}}{12}\right)}{\left(1 + \frac{PLR_{adj}^{(12)}}{12}\right)} \right)^{t} \tag{29}$$

where each rate *R* (*EE*, *MDF*, *PLR*) was converted from annual effective to monthly effective by

$$\frac{R_{adj}^{(12)}}{12} = \left[(1 + R)^{1/12} - 1\right] \tag{30}$$

These results are dictated in Table 3.8 and illustrated in Figure 3.11.

Table 3.8. Economic evaluation of the solar PV system installations for the highest energy generation per module and highest energy generation per region

Financial Aspects	Highest Energy Generation Per Module			Highest Energy Generation Per Region		
	$1.70/W	$3.57/W	$8.00/W	$1.70/W	$3.57/W	$8.00/W
Initial Capital Cost	$198,250	$309,800	$574,300	$496,000	$813,400	$1,507,600
Levelized Cost of Energy	$\frac{\$0.0793}{\text{kWh}}$	$\frac{\$0.1210}{\text{kWh}}$	$\frac{\$0.2197}{\text{kWh}}$	$\frac{\$0.8993}{\text{kWh}}$	$\frac{\$0.1371}{\text{kWh}}$	$\frac{\$0.2490}{\text{kWh}}$
Return on Investment	0.049%	-0.186%	-0.4730%	0.029%	-0.25%	-0.53%

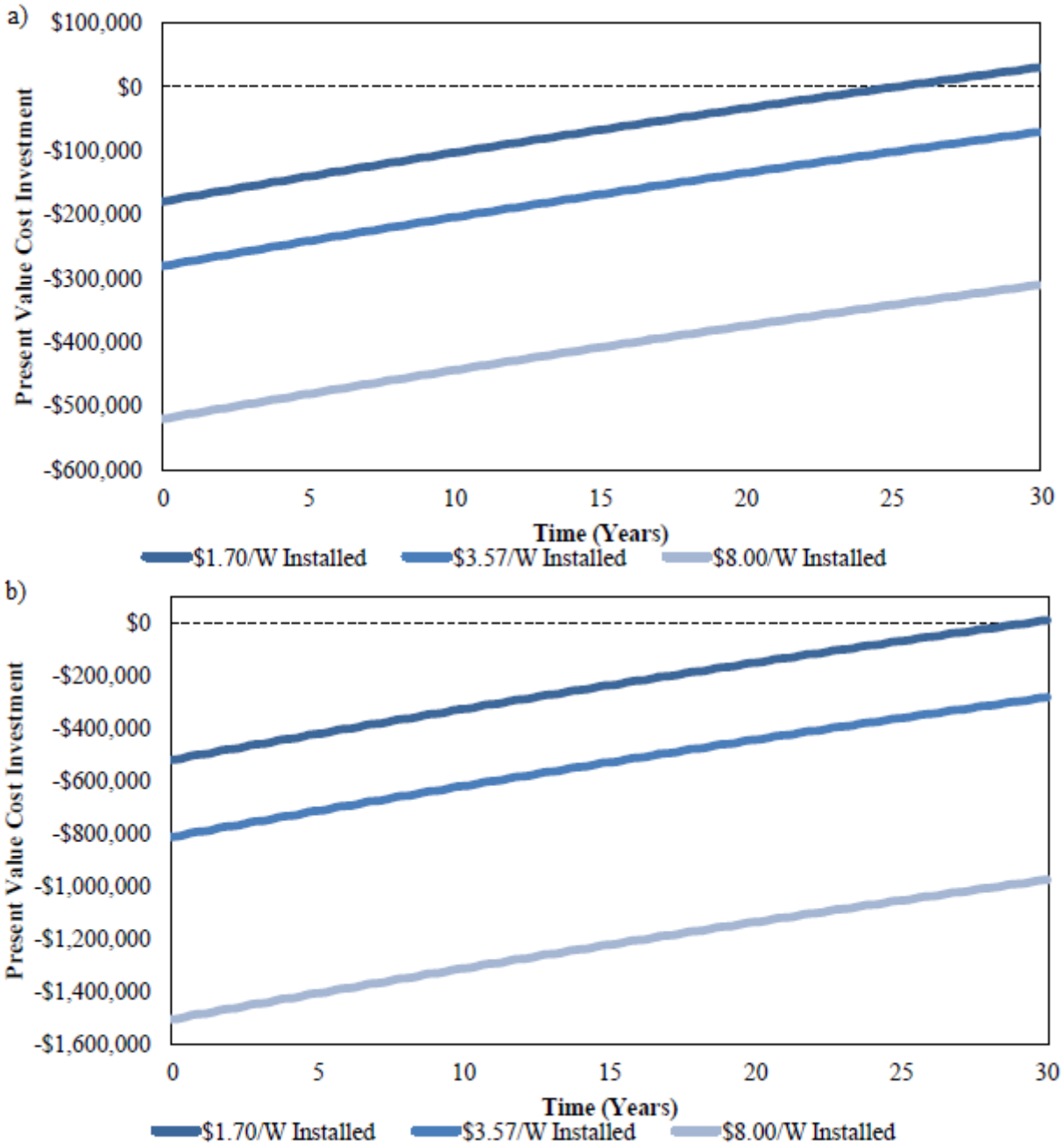

Figure 3.11. Economic evaluation of the solar PV system installations for a.) highest energy generation per module and b.) highest energy generation per region

Using these benchmark prices, an amortization schedule was created for 5, 10, and 15 year loans, where the initial downpayment is roughly 20% of the total installed cost. The monthly annuity *A* is determined by

$$A = \left(\begin{matrix}\text{Initial}\\ \text{Capital Cost}\end{matrix}\right) \cdot \frac{R_{adj}^{(12)}}{12} \Big/ \left[1 - \left(1 + \frac{R_{adj}^{(12)}}{12}\right)^{-n}\right] \tag{31}$$

where the interest rate *R* is the national prime lending rate. The payment summary is dictated in Table 3.9.

Table 3.9.Amortization payment summary for the solar PV system installations that correspond to the highest energy generation per module and highest energy generation per region

Financial Aspects		Highest Energy Generation Per Module			Highest Energy Generation Per Region		
		$1.70/W	$3.57/W	$8.00/W	$1.70/W	$3.57/W	$8.00/W
Initial Downpayment		$48,250	$64,800	$124,300	$101,000	$163,400	$307,600
Loan Amount		$150,000	$245,000	$450,000	$395,000	$650,000	$1,200,000
Payment (Monthly)	5 year	$2,708.83	$4,424.42	$8,126.48	$7,133.25	$11,738.25	$21,670.62
	10 year	$1,462.48	$2,388.72	$4,387.44	$3,851.20	$6337.41	$11,699.83
	15 year	$1050.55	$1715.90	$3,151.65	$2,766.44	$4552.38	$8,404.39
Total Interest Paid	5 year	$12,720	$20,776	$38,160	$33,496	$55,120	$101,760
	10 year	$25,894	$42,294	$77,683	$68,188	$112,208	$207,154
	15 year	$39,720	$64,877	$119,162	$104,597	$172,122	$317,765
Total Paid	5 year	$162,720	$265,776	$488,160	$428,496	$705,120	$1,301,760
	10 year	$175,894	$287,294	$527,683	$463,188	$762,208	$1,407,154
	15 year	$189,720	$309,877	$569,162	$499,597	$822,122	$1,517,765

3.8 Discussion

The results of the simulations are reasonably accurate on an annual basis; however, the discrepancies may be due to a variety of reasons such as the existing metered data being rounded, system shutdowns not being documented, and generally inconsistent weather patterns. Nonetheless, the solar tool may be improved in a number of ways. For instance, the algorithm for the module layout may be revised to account for pitched roof sections, or arrays at various module orientations. Whereas the simulation may be revised by including a detailed system thermal model, an inverter performance model, and losses in the conduit and connections.

In regards to the economic analysis, the 2013 US Solar Market Insight did not include the cost of labor, grid-interconnect, and permits, however these values were taken from 2010 bottom-up installed price benchmark and were adjusted based on their respective inflationary rate. The O&M and replacement costs were taken from a report that was made by Black & Veatch for NREL [61].As far as this tool having

the capabilities to reduce the installed costs, Michigan State University was quoted $50,000 for an evaluation of three rooftops of similar size to the case studies. However, this quote only examined one PV system design, whereas this tool can examine multiple PV system designs. In addition, the financial evaluation for the three rooftops would be an additional $30,000. That equates to almost $27,000 per roof. Therefore, this tool is a very cost-effective solution for any energy planner.

3.9 Summary and Conclusions

This section in the thesis describes a methodology for developing a parametric solar PV planning tool for grid-tied building applications that takes an adaptive modeling approach towards capitalizing on the complex geometry of a rooftop. The robustness of the tool was demonstrated and confirmed against existing PV systems, such that it may be utilized towards making the installation of a PV system more cost-effective.

Chapter 4 **FLUORESCENT TO LED LIGHTING RETROFIT**

Businesses, institutions, hospitals, etc. are always under constant pressure to reduce operational costs. Many estimates regarding commercial buildings, state that the lighting system accounts for roughly one-third of its total energy consumption, while more than half of the total energy consumption in retail and lodging buildings is attributed to the lighting system. However, it is all well documented that the lighting system has the largest potential for reducing a building's energy consumption [62].

A lighting system retrofit is defined as the practice of modifying or replacing an existing lighting fixtures, or luminaries with equivalent, more energy efficient accessories. This could be as simple as purchasing screw-in compact fluorescent lamps from a local hardware store to replace incandescent lamps, or a retrofit could be as in-depth as a detailed energy audit, engineering, feasibility study, and implementation. There are many benefits for retrofitting the lighting system, such as reduced labor and maintenance, reduced greenhouse gas emissions and non-monetizable benefits, which include productivity increase, and lower stress and anxiety. However, the largest benefit for retrofitting the lighting system is the energy savings over time [63, 64, 65]. Depending on the project size and complexity, there are roughly six phases in the retrofit process, which are highlighted in Table 4.1.

Table 4.1. Overview of the six steps for a successful lighting system retrofit

Phase	Rationale	Endeavors
Assessment	Make a quick assessment of the building lighting system	• Perform an initial walk-through of the building to assess the quality of lighting and potential for improvements
Data Procurement	Collect pertinent information needed for engineering	• Survey and document the existing lighting • Interview building occupants • Audit existing electric bills • Monitor existing lighting system

Engineering	Evaluate the current lighting situation, identify and suggest lighting retrofit opportunities, and evaluate cost effectiveness	• Evaluate current lighting quality
		• Evaluate current energy usage
		• Determine retrofit approach
		  ○ Relamp vs. redesign
		  ○ Occupancy sensors
		• Estimate retrofit costs based on approach
		• Estimate energy savings based on approach
		• Economic analysis

Procurement	Obtain cost information	• Bid construction company • Bid lighting retrofit products
Construction and Commissioning	Implementation	• Lamp and ballast disposal • Install retrofit equipment
Verification	Assessing the retrofit implementation to ensure assumptions	• Evaluate energy usage • Verify economics

In this chapter, an overview of each retrofit phase is provided, and is demonstrated with a case study on three building spaces around the campus of Michigan State University. The preliminary phase outlines key indicators for deeming if a lighting system retrofit is warranted. Next is a procedure for obtaining the pertinent energy usage and financial history is described. Then, an explanation about the main characteristics of light, along with a financial strategy for developing a series of retrofit options is explained. Subsequently, this leads into a brief overview about the procurement, construction, and design verification phase. Finally, this is concluded with a case study.

4.1 Phase I: Preliminary Assessment

The preliminary assessment phase is an evaluation of the current lighting technology in order to judge if a detailed lighting energy audit, engineering, and financial feasibility study is warranted. This step may be as simple as a phone call to the building manager, and reviewing the lighting blueprints and

utility bill history. On the other hand, it may consist of a building walk-though to survey the primary lighting technologies and lighting control devices. There are many indications to determine if a building will have a financially successful retrofit, some of which are listed in Table 4.2 [63, 64, 65].

Table 4.2. Indicators for determining the viability of an economically feasible retrofit

Economically Viable	Economically Unviable
• Contains energy intensive lighting • Contains lighting that was installed prior to 1980 • Long hours of operation • Eligible for incentives and rebates • High cost of energy • Current lighting technology is being discontinued • Lights remain on when a room is unoccupied	• Recently undergone a successful retrofit • Short hours of operation • Complies or exceeds ASHRAE/IESNA/ANSI 90.1, DOE, or LEED standards • Ineligible for incentives and rebates • Low cost of energy

4.2 Phase II: Data Procurement

If the project is considered financially viable for a lighting system retrofit, the subsequent procedure entails collecting information about the building. It is ideal to collect the data in an order mannered, such that the analysis is performed in an efficient fashion with minimal errors. The information being assembled is 1) the building schedule, which determines when the building is occupied; 2) interviews with building managers such that they can detail problem areas; 3) detailed inventory of the lighting equipment and size of each space; and 4) determining the lighting hours [64, 65].

4.2.1 Building Schedule & Utility Billing History

A building schedule is used to denote when the building is in operation. This is very advantageous when determining the energy usage that is spent when the building is occupied and energy that is wasted when the building is unoccupied. The total energy is used for determining if a lighting technology retrofit will be beneficial, or if occupancy sensors (O.S.) should be investigated. The energy used during operation is intended for assessing a lighting technology retrofit, and the energy spent when the building is unoccupied is used for appraising the feasibility of retrofitting a space for O.S [63, 64, 65].

The previous utility bills are used for determining when the peak power demand occurs, and correlate the peak demand with the commodity rate of electricity during peak usage. This is useful when calibrating the financial models for determining if a lighting system retrofit is financially viable [63, 64, 65].

4.2.2 Building Spaces & Inventory Survey

Well documented information about each space in the building, as well as a detailed inventory of the lighting system in each space is typically the most time consuming portion of the data procurement phase, but is essential for a successful retrofit analysis. In reference to Figure 4.1, the intent of this document is for detailing each building space. The floor level is meant for organization, whereas the space ID is unique for each space. The ASHRAE/IESNA/ANSI 90.1 room type is utilized for obtaining the proper lumens per watt based on the function of the room. The space dimensions are for calculating the appropriate lumens per watt, and the column for occupancy sensors is intended for detailing the energy usage [63, 64, 65].

Floor Level	Space ID	ASHRAE/ IESNA/ ANSI 90.1 Room Type	Space Dimensions			Currently Occupancy Sensors
			Ceiling Height	Length	Width	

Figure 4.1. Data input form for each space

In reference to Figure 4.2, this document is intended for detailing each type of fixture for each space. The type of fixture, housing, ballast, bulbs per fixture, and lumens per watt are intended for determining the lighting levels, and the most advantageous retrofit kit. As will be stated in Appendix III, different lighting technologies produce various light levels and energy consumption, which have a large effect on the engineering phase. Along with detailing each fixture, the conditions of the fixture were documented, for instance, the cleanliness and age of the lighting technology. In some cases, a light meter should be used for examining the current lighting quality and intensity [63, 64, 65].

Fixture							
Number of Fixtures	Type of Fixture	Type of Housing	Type of Ballast	Bulbs Per Fixture	Lumens Per Fixture	Watts per Bulb	Bi-Level or Single-Level Lighting

Figure 4.2. Data input form for each fixture for each room

4.2.3 Energy Audit

The economic viability is main driver for determining the success of a lighting system retrofit, where this success depends on the accuracy of energy audit. Due to not using submetering equipment for obtaining the energy usage, a procedure was developed, depicted in Figure 4.3, for obtaining the daily average energy usage. The procedure begins by using the raw data from the walk-throughs, and organizing it according to each perspective building space. Following, each building space was separated by the height of the ceiling. This was because at MSU has a different installation cost metric for fixtures above and below 15 feet had different installation costs. Then, each space was separated by whether or not an O.S. was present. Next, each type of fixture and the lighting level (bi-level, single-level) was separated. At this point, the procedure is split into sections. The first section determines the power consumption of each type of fixture based on the bulbs, lighting level, and driver/ballast power factor. The second section determines the average daily hours the lights are on in a space. This is established by separating the walk-though times by morning, afternoon, and night, where the times of day are dictated in Table 4.3.

Table 4.3. Walk-through times used to quantify energy usage

Time Period	Time of Day
Morning	8:00am-5:00pm
Afternoon	5:00pm-9:00pm
Night	9:00pm-8:00am

This is further separated by whether or not a room was occupied when the lights were on, which is used to determine the economics behind a feasible lighting control retrofit. From this organization process, the daily average energy consumption was determined.

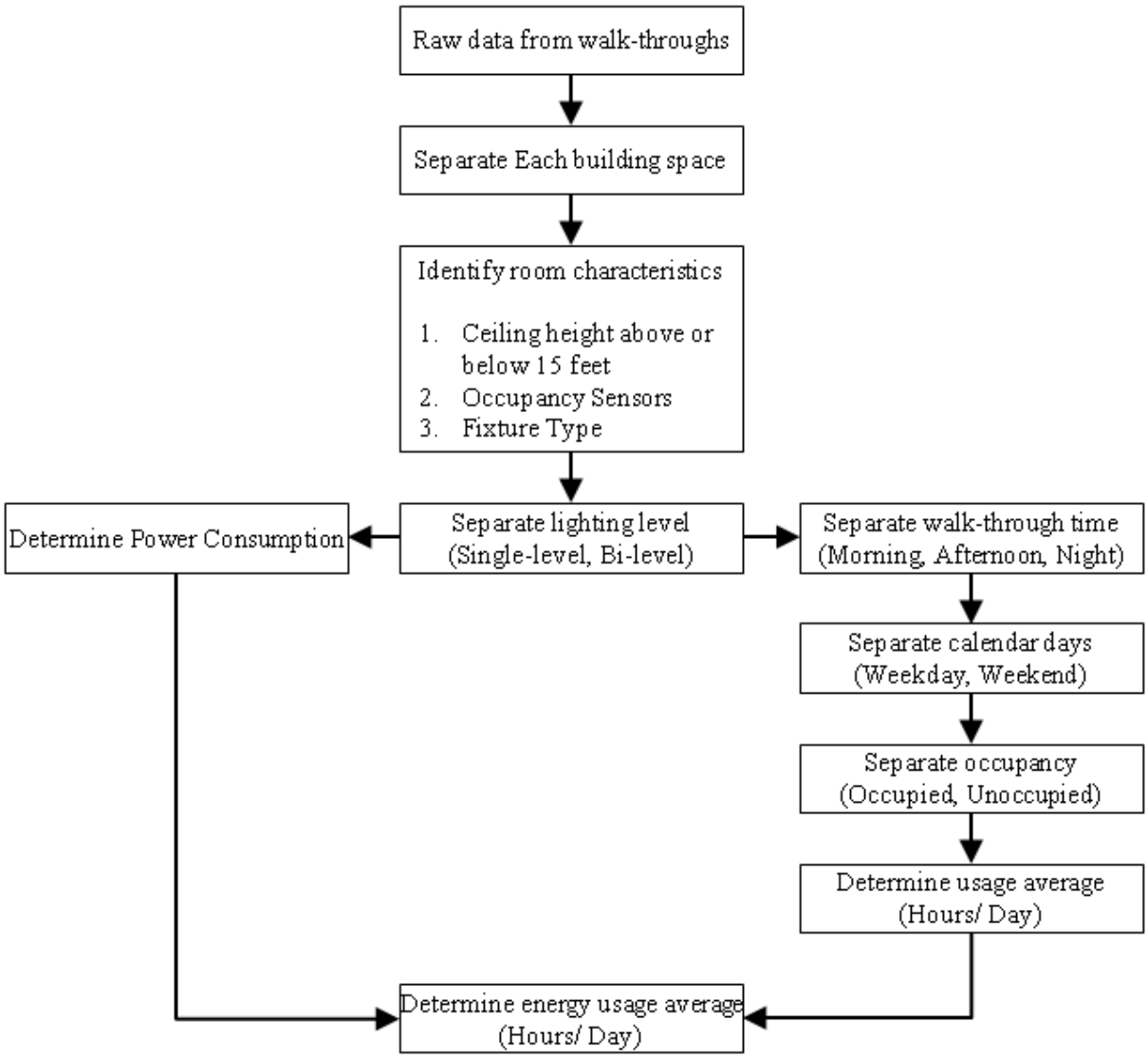

Figure 4.3. Flowchart for determining the average daily energy usage of each fixture

4.3 Phase III: Engineering

The engineering phase of the lighting retrofit involves evaluating the current lighting quality, and quantifying the current energy usage from the walk-throughs and inventory. From there, determining a series of options for approaching the retrofit, such as relamping with a retrofit kit or a complete redesign of the lighting system, as well as assessing the needs for occupancy sensors. Following, the economics of each retrofit option are analyzed, which is a culmination of the cost of the retrofit and the plausible energy savings.

4.3.1 Characteristics of Light

Light is defined as the portion of the electromagnetic spectrum that is visible to the human eye, where the radiant power emitted at each wavelength over this portion is the spectrum or the spectral power distribution. The spectra of a light source provides a complete description of a lamp's characteristics [63].

A light source's chromaticity is its quality of color, independent of illuminance, and is derived from the light source's spectra. The chromaticity chart, depicted in Figure 4.4, was created in 1931 by the Commission Internationale de l'Eclairage (CIE), where the *x* and *y* coordinates range from 0.0 to about 0.8, while the wavelengths corresponding to visible light are around the curved edge. For any given spectral power distribution, only one set of chromaticity coordinates exists. However, for any set of chromaticity coordinates, there is a variety of spectral power distributions. Often times, the chromaticity coordinates pertaining to the diagram are used to compare two or more colors for their respective appearance [63, 66].

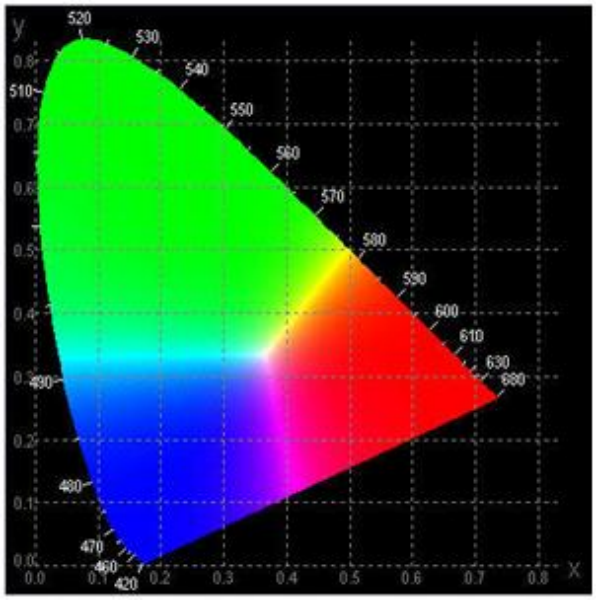

Figure 4.4. 1931 CIE chromaticity chart [63]

The correlated color temperature (CCT) is the apparent color of a light source in relation to a theoretical black body radiator. It is measured in Kelvins (K) and is derived from the spectra. Light sources with temperatures ranging from 3000 K or less, and have an orangish-yellow appearance are

considered to be “warm”. Whereas light sources with temperatures 4100 K or greater, and have a bluish-white appearance, are considered to be “cool” [63, 66]. The CCT chart is shown in Figure 4.5.

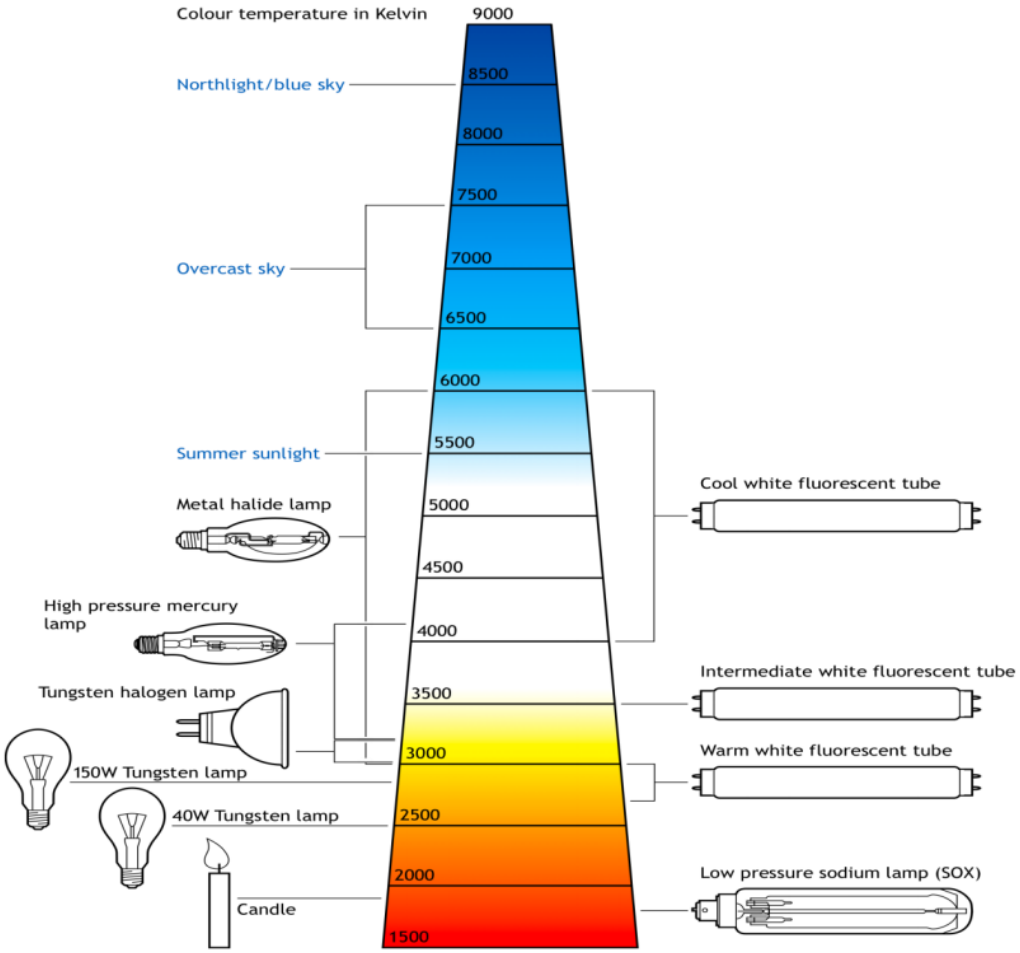

Figure 4.5. Color temperature chart courtesy of Sylvania Lighting

The CCT in a room has a dramatic affect on the occupants. For instance, a photographer usually prefers a very cool light that ranges from 4100-6500 K, whereas an office building prefers a neutral to cool light that ranges from 3500-4100. The IESNA preferred color temperatures are shown in Table 4.4.

Table 4.4. IESNA preferred color temperatures

Lamp CCT (Kelvin)	Application
<2500	Bulk industrial and security lighting
2500-3000 "Warm"	Used for low lighting areas (<10 footcandles) such as residential lighting, fine dining and family restaurants, and theme parks
2950-3500 "Neutral"	General feature lighting such as retail stores and galleries
3500-4100 "Cool"	General display lighting such as offices, schools, stores, industry, medicine, and sports
4100-5000 "Very Cool"	General work lighting such as offices, schools, stores, industry, medicine, and sports, as well as special applications where color is important
5000-7500 "Cold"	Special purpose lighting where color discrimination is very important

The color rendering index (CRI) is an additional property derived from the spectrum, and it is a general indicator of a light source's ability to reveal colors of objects in comparison to an ideal or natural light source. The CRI is a mathematical derivation that quantifies the shift in chromaticity when the light source is compared to eight specified pastel colors, depicted in Figure 4.6, where the amount of shift is ranked from 0-100, 100 being the best. For almost every application, a CRI of 80 should be the minimum [63, 66].

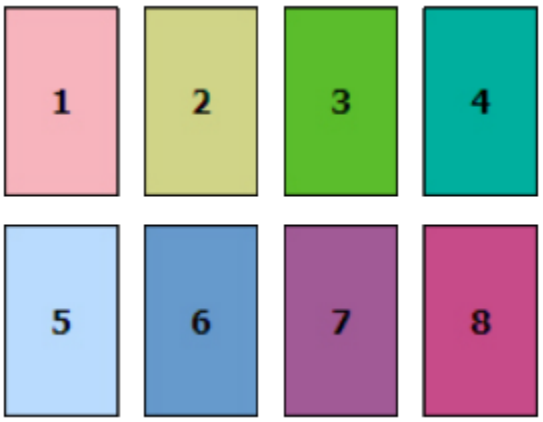

Figure 4.6. The IES eight pastel reference colors used for quantifying the chromaticity shift [64]

ASHRAE/ IESNA/ ANSI defines lighting power density *LPD* as the maximum watts of lighting per square foot of room floor area and is determined by [63, 67, 68]

$$LPD = \frac{fc}{LOE} \tag{32}$$

where *fc* is the illuminance (footcandles or lumens per square foot) that is assigned for the luminaries in the space. The light output effectiveness (*LOE)* is a function of the luminous efficacy *LE* (lumen output

per watt), a coefficient of utilization *CU*, and depreciation in the form of lamp lumen depreciation *LLD* and luminaire dirt depreciation *LDD*, and room surface dirt depreciation *RSDD*. The *CU* is a ratio of the lumen output to the room cavity ratio *RCR*, where the *RCR* is a relation between the fixtures height above a work plane (typically desk height), the room dimensions, and the type of space. [63, 67, 68] There is an assortment of *CU*'s, which can be found at [69]. The *LOE* is determined by

$$LOE = LE \cdot CU \cdot LLD \cdot LDD \cdot RSDD \tag{33}$$

In the ASHRAE/ IESNA/ ANSI 90.1 energy standards manual, two scenarios, whole building and space-by-space, are provided that characterizing maximum *LPD* [63, 67, 68]. Given that the approach we employed examined each individual space, we performed the analysis based on the space-by-space standard. A summary of the *LPD*s for common places around a university is provided in the Appendix II.

4.3.2 Retrofit Options

Typically, light sources are divided into two categories, natural and artificial. A natural light source is light from the sun and an artificial light source is from technologies such as incandescent lamps. In 2010, the U.S. commercial building sector estimated that 2.1 billion light fixtures were installed, which is approximately one-fourth of all installed fixtures in the U.S. The other light installations included the residential and industrial building sector. Depicted in Figure 4.7 illustrates the 2010 percentage of installed light fixtures in the U.S. commercial building sector [70].

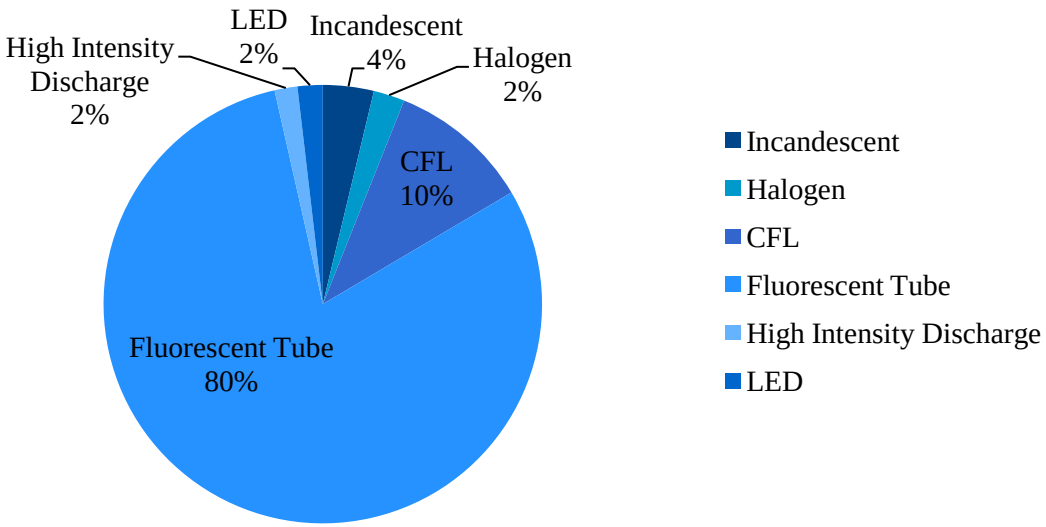

Figure 4.7. 2010 commercial building sector estimate of installed lamps technology

There is a copious amount of information available about the different types of lighting, which is highlighted in Appendix III.

When developing the retrofit options, assuming the initial system meets the *LPD* criteria, the first consideration taken into account was that Michigan State University wants a breakeven time-period of 3-5 years [71]. Therefore, the net present value *NPV* that incurs over the 3-5 year period is determined on a monthly scale, where the cash flows *CF* include the energy costs, replacement costs, O&M and each respective discount rate. The replacement time period *T* is determined by

$$T = \frac{\text{Lifetime of Current Technology (hours)}}{\text{Total Monthly Average Hours of Use}} \tag{34}$$

The basic *NPV* formula is

$$NPV = \sum_{t=0}^{T} CF \Big/ \left(1 + \frac{R_{adj}^{(12)}}{12}\right) \tag{35}$$

where *t* is the discrete time step. It should be noted the if the existing *LPD* was not up to current standards, this could result in either a complete redesign of the lighting system, or just a relamp.

The next step is evaluating the various types of lighting technology for their CCT, CRI, and *LPD*, and ensuring that each criteria is met. As stated earlier, the CCT and CRI can easily be obtained by using a spectrometer. Following each technology, if each characteristic has been met, will be evaluated using Eqs. (30), (34) and (36). Then, the technologies for each room that are deemed economically viable go through a bidding process.

4.4 Phases IV-VI

Phase IV, bidding the construction and material costs of the retrofit process, is dependent upon the size of the project. Typically these bids are then brought to the building owner or the board of directors, and they decide if the project should go into phase V, implementation. During implementation, the new retrofit equipment is installed and the former technology is disposed. Then phase VI is evaluating the retrofit to verify the energy usage assessment and economics [63, 64, 65, 67].

4.5 Case Studies

The retrofit design methodology is demonstrated on a classroom, a hallway, and an office. These building spaces experience long hours of operation, and they have the same F32T8 lighting technology that is soon to be discontinued [72]. Therefore, these areas are an ideal candidate for a retrofit.

The case studies are separated in two sections. The first section is a comparison of the current light quality characteristics to an LED retrofit option. When the various retrofit options were being determined, we were strongly encouraged by Michigan State University to examine LEDs. Consequently, a handful of LEDs were examined, but the LED that proved to have the least power consumption while still maintaining the desired light qualities is presented. The second section demonstrates the design methodology for obtaining the energy usage, and presents an economic evaluation. Additionally, the hallway walk-throughs were compared to metered data for the current lighting technology energy consumption and hours of usage.

Throughout Michigan State University, the most common lighting fixture is the 2x4 foot F32T8 3-lamp bi-level lighting troffer with a 0.87 ballast factor and a 0.98 power factor, which is also the only light fixture present in these building spaces. The lighting technology that is housed in the fixture has a 4100 K CCT and a 78 CRI.

4.5.1 Lighting Quality

For the three building spaces, the IESNA desired CCT is 3500-4200 K, and the preferred CCT by Michigan State University is 4000-4100 K. In addition, the CRI should be 80 at a minimum. When measuring the CCT and CRI based on the light sources spectra, there are two separate calculations. The first calculation utilizes the spectra to determine the CCT, whereas the second calculation, the CCT is declared in order to calculate a precise CRI. As mentioned previously, the CRI determines how close the light source is to its specified CCT.

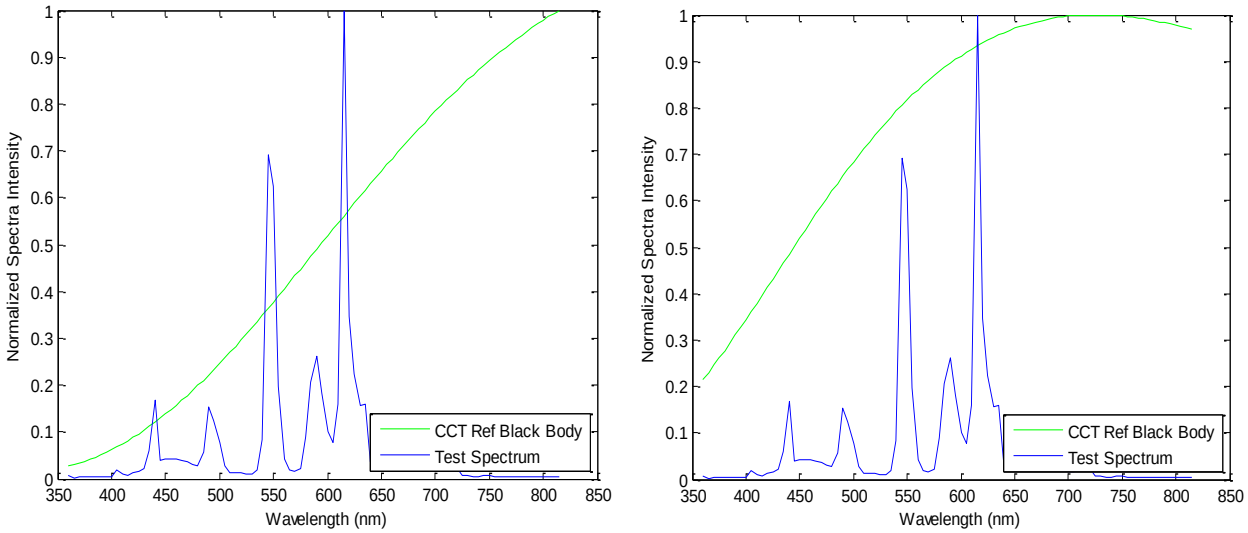

Calculate the CCT (measured) Declare the CCT (manufacturer)

Figure 4.8. The light quality tests for the current F32T8 bulbs. The CCT was measured off the spectra in a, and in b, the CCT was declared

The spectra along with the CCT in reference to a black body radiator for the current F32T8 lighting technology are depicted in Figure 4.8. When just the spectra was utilized, a CCT of 3700 K was determined, and when the CCT was fixed at 4100 K, according to the spec sheet, a CRI of 65 was found. These results are presented in Table 4.5.

Table 4.5. CCT and CRI parameter comparison of the current F32T8 lighting technology

Light Quality	Manufacturer	Measure Spectra to Calculate CCT and CRI	Declare CCT to Calculate CRI
CCT	4100 K	3700 K	4100 K
CRI	78	82	65

The spectra along with the CCT in reference to a black body radiator for the perspective LED lighting technology are depicted in Figure 4.9, When just the spectra was utilized, a CCT of 3800 K was determined, and when the CCT was fixed at 4000 K according to the spec sheet, a CRI of 87 was found. These results are presented in Table 4.6.

Table 4.6. CCT and CRI parameter comparison of the perspective LED technology

Light Quality	Manufacturer	Measure Spectra to Calculate CCT and CRI	Declare CCT to Calculate CRI
CCT	4000 K	3800 K	4000 K
CRI	80	84	87

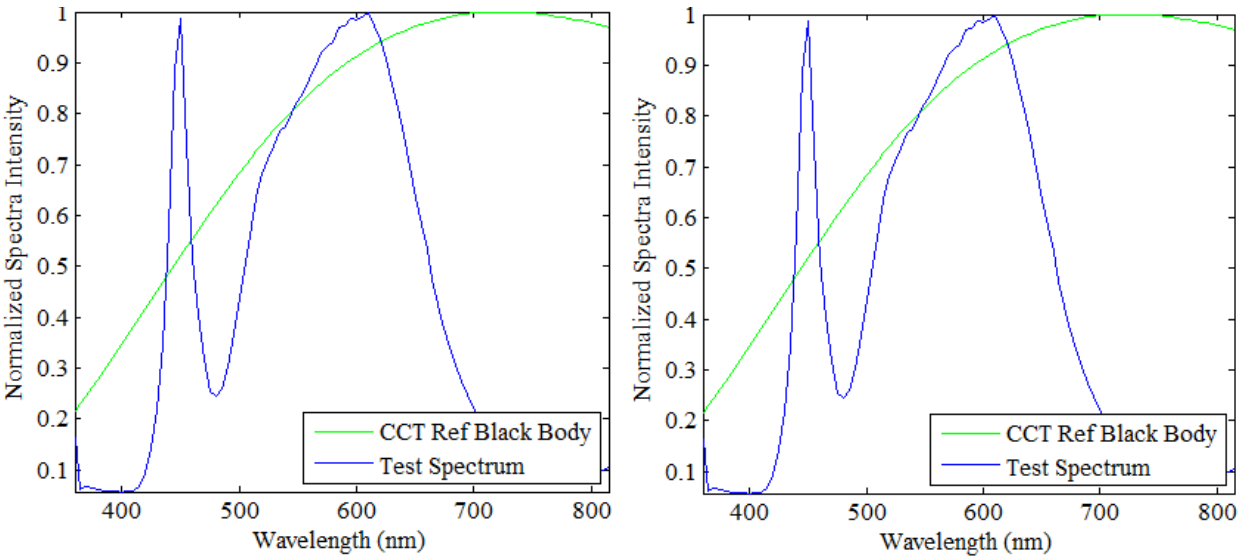

Calculate the CCT (measured) Declare the CCT (manufacturer)

Figure 4.9. The light quality tests for the perspective LED retrofit kit. The CCT was measured off the spectra in a, and the CCT was declared in b

While the lighting quality characteristics of the LED lighting technology are similar to the current F32T8 lighting technology, a side-by-side comparison exhibits the validity of Michigan State University utilizing LEDs throughout the campus.

Current F32T8 lighting technology Perspective LED technology

Figure 4.10. Side-by-side color comparison, where the current F32T8 lighting technology is shown in a, and the perspective LED lighting technology is shown in b

4.5.2 Financial Feasibility Study

The financial feasibility of the retrofits was analyzed by using the traditional NPV project evaluation. The *NPV* was calculated by culminating the specifications and capital cost of the two lighting technologies, along with the expected annual hourly usage that pertains to each building space. Table 4.7 exhibits a feature comparison of the current lighting technology to proposed LED retrofit technology, and Table 4.8 portrays the annual usage hours for each building space. The annual usage hours were calculated by following the procedure outlined in Figure 4.3, where if the lights were on at single-level, they were normalized to bi-level for comparative purposes.

Table 4.7. A comparison of the two lighting technologies that are being assessed for the financial feasibility of a retrofit

Light Characteristics	Current Fluorescent Lighting Technology	Perspective LED Lighting Technology
Anticipated Lifetime (Hours)	24000	50000
Peak Power Consumption (Watts)	97.5	45
Capital Cost	$6.51	$110
Efficacy (Lumens/Watt)	61.6	88.9

Table 4.8. Estimated hourly usage on an annual basis

Space	Amount of Fixtures	Usage (Hours)	
		Walk-throughs	Metered Data
Classroom	16	3830	
Hallway	12	8650	8425
Office	12	5840	

Then by following the procedure illustrated in Figure 4.3, for sorting through the raw data from walk-throughs, the annual energy use for the current lighting technology, including classroom, hallway, and office is 4480 kWh, 10120 kWh, and 6830 kWh, respectively. The annual energy cost for the classroom, hallway, and office is $585, $990, and $670, respectively, and the replacement period for those same locations are 6.3 years, 2.8 years, and 4.1 years respectively. Whereas, for the LED Retrofit Kit, the annual energy use for the classroom, hallway, and office is 2050 kWh, 4640 kWh, and 3130 kWh respectively. The annual energy cost for the classroom is $265, hallway is $450, and office is $305. The replacement period, in years, is 13, 5.8, and 8.5, respectively.

Table 4.9. Financial characteristics for the lighting retrofit of the three building spaces

Financial Characteristics	Current Lighting Technology			LED Retrofit Kit		
	Classroom	Hallway	Office	Classroom	Hallway	Office
Annual Energy Use (kWh)	4480	10120	6830	2050	4640	3130
Annual Energy Cost	$585	$990	$670	$265	$450	$305
Replacement Period (years)	6.3	2.8	4.1	13	5.8	8.5

As depicted in Figure 4.11 and shown in Table 4.10, the classroom breakeven time period, in years, is 6.0, while the office is 3.8, and the hallways is 2.5. The amount saved over the lifetime of an LED Retrofit Kit is $2175 for the classroom, $1731 for the office, and $1806. The payoff system and return on investment in the classroom is 111%, for the office is 119%, and for the hallway is 124%. The return on the investment period in the classroom, office, and hallway is 13.1 years, 8.6 years, and 5.8 years respectively. The CO_2 reduced was based on the $6.9x10^{-4}$ metric ton of CO_2/kWh [73].

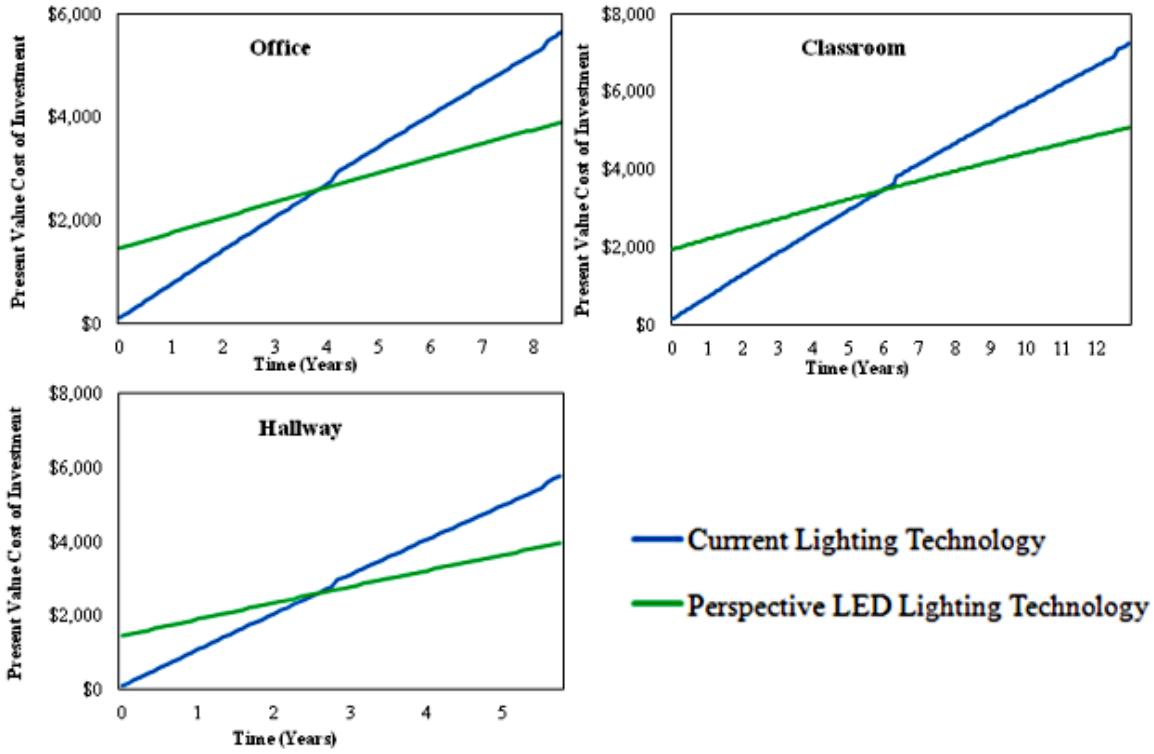

Figure 4.11. Economic evaluation of the three building spaces. The breakeven time period is where the current lighting technology intersects with the proposed LED technology

Table 4.10. Economic feasibility comparison of the two lighting technologies

Financial Characteristics	Classroom	Hallway	Office
Break-Even Time Period (Years)	6.0	2.5	3.8
Amount saved over lifetime of LED Retrofit Kit	$2175	$1806	$1731
Return on Investment	111%	124%	119%
Return on Investment Period (Years)	13.1	5.8	8.6
CO_2 Reduced Over Lifetime of LED Retrofit Kit (Metric Tons)	17.2	12.9	12.9

4.6 Discussion

The breakeven time period, amount saved, and return on investment were based on the energy savings in comparison to the current lighting technology. This analysis included the capital cost of the LED retrofit kit, installation and installation materials such as wire. Furthermore, the replacement costs of the current technology, labor, and commodity rate of electricity were calculated at a fixed rate and adjusted for their respective inflation. The labor rates were provided from Spencer Speerbreaker, a Master Electrician at Michigan State University, where each building space scenario was categorized on a fixture basis for the time required for installation, number of laborers (master electricians and apprentices) as well as equipment need such a scissor-lift, ladder, or scaffolding. The degradation of the each lighting technology in regards to energy consumption was not included. It should be noted this office under study was a graduate student office, and typically these offices experience longer than normal periods of use. The energy consumption of the current and perspective lighting technology was gathered using metered data. However, the logged usage data for the hallway was not included in the financial analysis because of large outlier values being present throughout the data.

4.7 Summary and Conclusions

The results of the case studies demonstrate that LED technology not only reduces energy costs, but also has a noteworthy return on investment and a substantial reduction in greenhouse gas emissions. While the classroom analysis may not fall in MSU's desired range for a retrofit, it is clear that this office and hallway are economically viable.

APPENDICES

Appendix I: Solar Photovoltaic Time Periods

The financial analysis for solar PV was performed on a monthly basis, where the warranty and replacement time periods are based on industry norm [74]. Table A.1 depicts the initial capital costs, which occur at time 0. Additionally, the inverter's warranty expires after five years, and typically needs replacement every ten years. The warranty on the modules and the disconnect switches are 25 years, but are expected to be able to last up to the industry norm of 30 years, which is the length of the solar PV project analysis. In our analysis, we assumed that it would take one month to install a rooftop solar PV system.

Table A.1. Time periods for BoM and expected periods for replacement

Time (Years)	0	5	10	15	20	25	30
Modules	X					Warranty Expires	
Mounting System	X						
Storage	X						
Inverter	X	Warranty Expires	X	Warranty Expires	X	Warranty Expires	
Tracker	X						
Combiner Boxes	X					Warranty Expires	
Meter	X						
System Monitor	X						
DC-AC Switch	X					Warranty Expires	
Fuses and Holders	X						
Wires, Conduit, Nuts, Bolts, etc.	X		X		X		

Table A.2 depicts the construction labor time periods. The construction labor time periods follow directly in line with the Table A.1 for initial capital costs and replacements of components.

Table A.2. Time Periods for Labor Costs and Expected Periods for Replacement

Time (Years)	0	5	10	15	20	25	30
Electrical	X		X		X		
Hardware	X		X		X		
Overhead	X						
Profit	X						

Table A.3 depicts the indirect capital costs. All of these costs occur during the construction stage of the project, and sales tax is applied for when the inverter is being replaced. The land cost and site prep is considered to be $0.00, because MSU owns its buildings and being that MSU has 110+ buildings, they can choose the building that needs minimal preparation.

Table A.3. Indirect capital costs time period

Time (Years)	0	5	10	15	20	25	30
Permitting & Commissioning	X						
Grid Interconnect	X						
Land	X						
Site Prep	X						
Sales Tax	X		X		X		

Table A.4 depicts the discrete indirect costs. The maintenance and cleaning costs is largely due to cleaning, which should be performed monthly. Additionally, the Chairs at MSU's Infrastructure & Planning Facilities requested that we account for insuring the system, and that they are billed monthly, as well as a fund for inverter replacement such that they are able to prepare for these costs.

Table A.4. Discrete indirect costs

Time (Years)	0	5	10	15	20	25	30
Maintenance and Cleaning		X	X	X	X	X	X
Insurance		X	X	X	X	X	X
Inverter Replacement Reserve		X	X	X	X	X	X

Table A.5 depicts the trend in a module. The module produces energy every day, but experiences a degradation in the power generation capabilities.

Table A.5. Module time periods

Time (Years)	0	5	10	15	20	25	30
Panel Degradation		X	X	X	X	X	X
Energy Generation		X	X	X	X	X	X

Appendix II: Lighting Power Density for Common Spaces Around a University

Table A.6. The ASHRAE/ IESNA/ ANSI 90.1 LPD for the common space types around a university

Common Space Type	LPD (W/ft^2)	RCR Threshold
Atrium		
First 40 ft in height	0.03 per ft (height)	NA
Height above 40 ft	0.02 per ft (height)	NA
Audience Seating Area - Permanent		
For Auditorium	0.79	6
For Performing Arts Theatre	2.43	8
For Motion Picture Theatre	1.14	4
Classroom/Lecture/Training	1.24	4
Conference/Meeting/Multipurpose	1.23	6
Corridor/Transition	0.66	Width<8ft
Dining Area	0.65	4
For Bar Lounge/Leisure Dining	1.31	4
For Family Dining	0.89	4
Dormitory	0.38	8
Dressing/Fitting Room for Performing Theatres	0.40	6
Electrical/Mechanical	0.95	6
Food Preparation	0.99	6
Laboratory		
For Classrooms	1.28	6
For Medical/Industrial/Research	1.81	6
Lobby	0.90	4
For Elevator	0.64	6
For Performing Arts Theatre	2.00	6
For Motion Picture Theatre	0.52	4
Locker Room	0.75	6
Lounge/Recreation	0.73	4
Office		
Enclosed	1.11	8
Open Plan	0.98	4
Parking Garage	0.19	4
Restrooms	0.98	8
Stairway	0.69	10
Storage	0.63	6
Workshop	1.59	6

Appendix III: Lighting Technologies

A.III.1 Daylight

Daylight is the combination of direct and indirect sunlight that is utilized to illuminate a room via a window or skylight. When daylight is employed in a building, a delicate balance between the HVAC system and the solar heat gain must be considered. Certainly, using daylight in comparison to artificial lighting has significant energy savings in regards to the lighting system. However, a room that uses daylight during the warmer months will inevitably experience solar heat gain, which in turn creates a higher demand on the HVAC system to cool the room. Thus ensuing a delicate balance of daylight to the HVAC energy demand.

Nonetheless, daylight is the most desirable light source in a building because of excellent characteristic properties, as well as providing psychology benefits to occupants. Daylight has a CCT of 6500, a CRI of 100, and is a full spectrum light source, thus meaning it covers all wavelengths of the visible light spectrum, or all wavelengths that are useful to plant and animal life. Thus, many artificial light sources should roughly mimic the same properties of daylight [63, 67, 75].

A.III.2 Incandescent Light

Thomas Edison invented the incandescent light bulb in 1879. The incandescent bulb, shown in Figure A.1, is comprised of a very fine tungsten filament wire, sealed by a glass bulb, and filled with argon gas. When electrical current passes through the filament, the filament will heat up and emit light. This technique converts five to ten percent of the energy into light, and the rest is emitted as heat [67, 76].

Figure A.1. Typical incandescent light bulb

In 2010, the incandescent lamp was the most common light bulb in all lighting applications. It accounted for roughly 62% of installed lights in residential applications, but only 4% in non-residential applications. The reason behind this dramatic installation difference in the various building sectors is due to a recent DOE bill, which was created to phase out the use of these bulbs in non-residential applications [70, 77].

There are many advantages to the incandescent lamp. The main advantage is the relatively low capital cost, dimming capabilities and no need for extra equipment such as a ballast. Additionally, the incandescent lamp has a CRI of 100 and a CCT that ranges from 2400-2900 K. However, there are many disadvantages as well. Roughly 5-10% of the electrical energy input produces light and the rest is emitted as heat. This heat gains leads to the building's HVAC equipment working more often. Furthermore, in comparison to other artificial lighting technology, the incandescent lamp is the least luminous, 12-18 lumens per watt, and has a lifetime of 750-1,500 hours [63, 78].

A.III.3 Halogen Lights

The halogen lamp, shown in Figure A.2, is much like the incandescent lamp. They both have a tungsten filament, but the halogen lamp contains bromine and iodine gas encased in quartz at a pressure of 7-8 atm, as compared to argon gas encased in glass. The halogen lamp produces light via the halogen cycle. The cycle starts by passing an electrical current though the filament. This causes the filament to heat up and release tungsten atoms. At moderate temperatures, the tungsten atoms will chemically unite with the halogen gas, thus creating a halide. At higher temperatures, the halide will dissociate, which releases tungsten atoms and frees the halogen atoms to repeat the process[66, 76].

Figure A.2. Typical halogen light bulb

In 2010, the halogen lamp accounted for 4% of installed lights in residential applications, and 2.3% of commercial applications [70]. One reason behind the small market percentage is the type of

applications used for this technology. Halogen lamps, known for high luminous output, are typically used in stadium lights, work lights, and film lights [63, 76].

The main advantage is the relatively low capital cost, dimming capabilities no need for extra equipment, such as a ballast, and no warm up time. Additionally, the halogen lamp has a CRI ranging from 95-100, a CCT that ranges from 2800-3400 K, and an efficacy of 16-29 lumens per watt. Furthermore, the lifetime of the lamp varies due to on-off cycles, but statistically has a lifetime of 2,000-4,000 hours. However, there are many disadvantages as well. The halogen lamp becomes extremely hot and easily capable of causing severe burns. In addition, this lamp is sensitive to oils left behind from human skin. These oils when heated up can cause imbalance, resulting in possible rupture of the bulb [63, 76].

A.III.4 Fluorescent Light

The fluorescent lamp contains a mixture of argon gas and mercury vapor, sealed by a glass tube. This glass tube has a phosphorous coating on the inside wall, and at each end of the glass tube, there are two electrodes wired into an electrical circuit. When electrical current flows to the electrodes, it creates a substantial voltage across at each electrode. This causes electrons to migrate through the argon gas from one end of the tube to other. In doing so, some of the mercury in the tube changes from liquid to gas. When electrons and charged atoms collide with the gaseous mercury atoms, the electrons of mercury atoms become excited and jump to higher energy levels. When the electrons return to the original energy level, they mainly release photons in the UV wavelength range. When these photons encounter the phosphor atoms, it causes the phosphor atom to be bumped to a higher energy level. When the photon returns to its original position, energy is released in the form of another photon, which also releases white light. The color of the light is varied with different phosphor combinations. The typical fluorescent lamps CCT range is 2,700-6,500K and CRI range is 80-90 [76].

For this thesis, the fluorescent lamp is divided into two parts. The first part describes the compact fluorescent light (CFL), and the second part describes the fluorescent tubular light.

A.III.4.1 Compact Fluorescent Light

The compact fluorescent light (CFL), shown in Figure A.3, is one alternative to incandescent lamps. In 2010, the CFL accounted for 23% of installed lights in residential applications, and 10% of commercial applications [70]. The reason behind this dramatic installation difference in the various building sectors is due to that most applications for CFLs are for specialty decorative applications [63, 76].

Figure A.3. Typical compact fluorescent light bulb

The greatest advancement in CFL technology is the built-in electronic ballast. Originally, the CFL contained a magnetic ballast, which created an unpleasant buzzing sound, and a long startup time [79].

The main advantage to using CFLs is that it can replace almost any incandescent lamp with little to no change to the fixture, and it is relatively inexpensive. Additionally, in comparison to the incandescent lamp, the CFL has an expected lifetime 13 times greater, and requires 80% less electrical energy to produce the equivalent amount of light [76]. However, the main disadvantage of CFLs is that they contain mercury, a highly toxic chemical. If any bulb is broken, one should take steps to expel the gas in that room. However, some hardware stores offer CFL recycling at no charge to the customer. The other disadvantage is that not all CFLs can be dimmed, or designed for rapid on/off switching [78].

A.III.4.2 Fluorescent Tubular Light

The fluorescent tubular lamp, sometimes referred to as linear fluorescent lamp is shown in Figure A.4. In 2010, the fluorescent tubular lamp accounted for 29% of all artificial light applications, where

10% was for residential applications, and 80% was for commercial applications. The reason behind this dramatic installation difference in the various building sectors is due to that most applications for fluorescent tubular lamps are for lighting applications compared to aesthetics [63, 76].

The rectangular and strip fluorescent tube fixtures, containing one to four lamps, are the most common in commercial applications. Until the 1980s, the standard lamp was the T12 lamp in 4 and 8-foot lengths, whereas today the most common lamp is the T8. In the fluorescent lighting nomenclature, the "T" designation stands for tubular, the shape of the lamp. The number following the T gives the lamps diameter in eighths of an inch. Thus, the diameter of a T12 lamp is twelve-eighths of an inch, or one-and-one-half inches. When comparing the light output of the T8 and the T12, the T8 has roughly 10% more light output per watt [79].

The fluorescent lamp has the same design principles as the CFL, except the ballast is separate from the actual lamp. Therefore, this allows for large amount of flexibility of lamp and ballast combinations for designing a room. Fluorescent lamps are very energy efficient in comparison to incandescent lamps, where fluorescent lamps use 85% less energy, and offer a lifetime of about 20,000 hours. The main disadvantage for fluorescent lamps is the constant flickering. The flickering leads to health effects of the occupants, such as headaches and eye strain [63, 79, 76].

Figure A.4. Typical fluorescent tube light

A.III.5 Light Emitting Diodes LED

As far as energy efficiency and LPW, the LED lighting technology is considered the best alternative to incandescent lamps. However in 2010, less than 1% of residential applications and less than 2% of commercial applications used LEDs. These low numbers are largely due to the high capital cost of the light during 2010, which was about $1.71/klm as compared to today, where the cost is about $0.97/klm. Also from 2010 to 2012, the market has seen a 350-3,500% installation growth rate, depending on the type of LED bulb [70, 80].

The LED lamp, unlike incandescent, halogen, and fluorescent lights, is based on solid-state lighting (SSL) technology. The term SSL refers to light emitted by electron movement in a semiconductor material. To further explain this, a diode consists of doped semiconducting chips to create a p-n junctions. When current flows across the p-n junction, the n-side releases electrons and meet holes on the p-side. In doing so, the electrons fall into a lower energy level and release energy in the form of a photon .

The main advantages of LEDs are they consume 10-30% less energy to produce the same amount of light. They also have a lifetime of about 50,000 hours and a CCT ranging from 2,700-5,000K and a CRI range of 70-95. The main disadvantage is the capital cost of LEDs. This is main deterrent for switching over to LEDs. Also generally the CCT and CRI is much hotter than what most prefer. But, this is also a hot-topic of R&D [76].

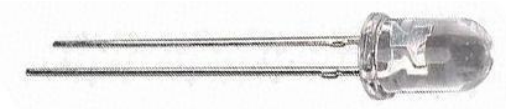

Figure A.5. Typical LED diode

Appendix IV: Economic Fundamentals

This section provides an overview of a few elementary financial terminologies such as cash flows, interest rates, time periods, discount rates, expected present value, taxes, system depreciations, and fixed charge rates. As well as, this section describes capital budgeting techniques for net present value, whole-life cost, internal rate of return, and levelized cost of energy.

A.IV.1 Cash Flows

The cash flows are the most important economic analysis for almost any investment. The cash flows for our project analysis can be broken up into 3 main components, which are: 1) overnight cost of capital; 2) discrete indirect costs; and 3) accrued energy savings. The overnight cost of capital accounts for all the components of a project, as well engineering, labor, land and project overhead. The monthly discrete costs include O&M, unscheduled maintenance, component replacement reserve, insurance and property taxes. The component replacement reserve for a solar PV project is the inverter, whereas for a lighting system retrofit project, this could be a driver for a LED or a power pack for an occupancy sensor. The accrued energy saving for a solar PV system is a function of the amount of energy generated from the PV system, and the commodity rate of electricity from the power plant. The accrued energy savings from lighting system retrofit is a function of the reduced amount of energy from lighting as compared to the current technology, and the commodity rate of electricity from the power plant .

A.IV.2 Interest Rates

The cash flows can be expressed either in current dollars or in constant dollars. Current dollars are defined as actual cash flows observed in the market, and change in value over time due to inflation and or escalation, i.e. a dollar today is not worth the same as a dollar tomorrow. Constant dollars are defined as the dollar worth at the base year. Constant dollars values do not take into account inflation and or escalation, and therefore not considered in the financial analysis. The current dollar equation of a cash flow is

$$CDCF = \frac{CF_t}{(1+e)^t} \quad (36)$$

Where *CDCF* is current dollar cash flow, CF_t *i*s cash flow at time *t*, *e* is the interest rate, and *t* is time [81].

There is a multitude of inflation rate indices, such as Consumer Product Index (CPI), Gross Domestic Product (GDP), and Producer Price Index (PPI). The CPI is the most widely followed inflation measure, and measures the average change in price, in prices of a market basket of consumer goods and services, and price trends at the retail level. The CPI for the United States, as defined by the Bureau of Labor Statistics, is "A measure of the average change over time in the prices paid by urban consumers for a market basket of consumer goods and services". The national CPI is calculated monthly from the average change in price of goods, which included in the basket, for 85 separate locations. The GDP is the market value of the national output of goods and services, in a given period of time. The GDP per capita is typically recognized as an indicator of a country's standard of living. The movement of the GDP often closely mimics the CPI [81].

A.IV.3 Time Periods

The time period of a cash flow is imperative for any financial analysis. The most important time periods from a reporting standpoint is the base year, dollar year, and investment year. The cash flows from each time period are converted to the base year, sometimes called year zero. The dollar year is at a different period than the base year, which could be past or future. The dollar year is converted to the base year by using its respective interest rate and the number of periods from the base year. The investment year is the year when the investment occurs [81].

Other important time periods for a financial analysis include the lifetime of the investment *L*, the analysis period *N*, the depreciation period *M*, the finance period *Y*, and the levelization period *P*. The lifetime of the investment is an estimate of the useful lifetime of an investment. The typical lifetime for a solar PV system's is 30 years, and a LED bulb is 50,000 hours. The analysis period is a period of time that an investment is being evaluated. The depreciation period, which is particularly important for tax

purposes, is the period of time an investment is amortized. The finance period, sometimes referred to as the loan period, is the period of time for which finance is structured. The levelization period is the period of time used for calculating the levelized cash flow stream. In a financial analysis, the time points selected are generally equally, i.e. yearly or monthly, but could different [81].

To summarize time periods with an example, let's say a solar PV system started construction in 2010, but the construction took two years to complete. Therefore, the base year is 2010, which is when all the initial capital costs took place. The project goes into service in 2013, and any cash flows from 2013 on, need to be converted to the base year of 2010. Some of these cash flows occur monthly, such as O&M, while others occur many years since operation, such as replacing the inverter. However, all of these cash flows need to be converted to the base year of 2010.

Selecting a time and analysis time period is essential. If reporting cash flows, without reporting the base year, the data is useless. Many times in practice, the investments lifespan is equal to the analysis period.

A.IV.4 Discount Rate

The well known saying that, "a dollar today is worth more than a dollar tomorrow", typically referred to as the time value of money, is because a dollar received today can be invested to earn interest immediately. The discount rate acts as a measure of the time value of money, and is pivotal to the present value calculation. The discount rates may be viewed as inherent risk of an investment. In this analysis, we consider the prime lending rate from a bank as the discount rate, because it may be viewed as the opportunity or risk of investing in project vs. investing the money in a bank [81].

A.IV.5 Depreciation, Tax Rates, and Renewable Energy Tax Credits

Depreciation is the reduction in value of assets, and is a tool for recovering the cost of assets via an income tax deduction. Depreciation is strictly an accounting detail and does not involve cash flows, or the deterioration of the physical asset. The depreciable base is the capital sum that may be recovered by depreciation, and the adjusted base is when the depreciable base is adjusted annually by the depreciable

amount [81]. However, Michigan State University is a public university that typically holds onto an investment past its useful life, and is tax exempt. Thus, depreciation, renewable energy tax credits and all tax rates, with the exception of sales tax, are not considered.

A.IV.6 Expected Present Value

Expected present value analysis is the anticipated current worth of a future cash flow stream, converted to the base year, given a specified rate. In other words, expected present value is today's value of future cash flows. Expected present is one of the most fundamental and important analysis tools for any investment. When calculating the expected present value, it is essential to keep track of constant or current dollars. Real discount rates must be used with constant dollars, and nominal discount rates, which include inflation, must be used with current dollars [81].

The basic expected present value equation $\mathbb{E}pv$, of a cash flow CF_t, occurring at time t, with a discount rate d is

$$\mathbb{E}pv = \frac{CF_t}{(1+d)^t} \tag{37}$$

An annuity immediate is a periodic cash flow of fixed size, for example, routine O&M. The expected present value of an annuity immediate with interest rate i, and n cash flows is

$$\mathbb{E}pv = CF_t * \frac{1-(1+i)^{-n}}{i} \tag{38}$$

A.IV.7 Net Present Value

The most widely accepted financial method to determine the profitability of an investment is the net present value *NPV*. It examines the difference between the present value cash inflows, sometimes called revenue, and the present value of cash outflows, sometime called costs. The *NPV* is sensitive to the reliability of an investment, because it takes into account inflation and discount rates. A project that has a positive *NPV* is a viable investment. The *NPV* formula, where CF_t, is the cash flows at time t, and r is the various rates, is

$$NPV = \sum_{t=1}^{T} \frac{CF_t}{(1+r)^t} \tag{39}$$

A.IV.8 Whole-Life Cost

The whole-life cost *WLC*, or life-cycle cost are the costs sustained during the ownership of the project. This includes the initial capital costs, indirect costs, discrete costs, etc. The *WLC* analysis is a well-defined procedure to estimate the overall present value costs of a project, and compare the results to alternatives [81].

A.IV.9 Internal Rate of Return

The internal rate of return *IRR* is a capital budgeting calculation for comparing the profitability of a project. The internal rate of return is the rate of return that makes the net present value of all cash flows for a particular investment equal to zero. *IRR* is not recommended for rating mutually exclusive projects, but should rather be used when deciding if a single project is worth investing into [81]. The *IRR* is found by solving the polynomial developed in

$$Npv = \sum_{t=1}^{T} \frac{CF_t}{(1 + IRR)^t} = 0 \tag{40}$$

A.IV.10 Levelized Cost of Energy

The levelized cost of energy *LCOE* is a calculation that compares the cost of energy from different fuel sources. In our case, the *LCOE* is the cost of energy generated from a solar PV system. The *LCOE* includes the entire present value system costs, such as initial capital, loan payments, O&M, etc. This type of calculation creates a comparison, which helps guide decision makers [81].

BIBLIOGRAPHY

BIBLIOGRAPHY

[1] U.S. Energy Information Administration, "Monthly Energy Review April 2014," U.S. Department of Energy, Washington D.C., 2014.

[2] P. Thakur, S. Ballard and R. Nelson, "Radioactive Fallout in the United States Due to the Fukushima Nuclear Plant Accident," *Journal of Environmental Monitoring,* no. 5, pp. 1317-1324, March 2012.

[3] G. Liu, B. Liu, W. Wang, J. Zhang and R. Athalye, Advanced Energy Retrofit Guide - Practical Ways to Improve Energy Performance, Richland, Washington: Department of Energy, 2011.

[4] J. Kelso, "2007 Buildings Energy Data Book," Silver Spring, Maryland: D&R International, Ltd, 2007, pp. 1.1-1.17.

[5] The Franklin Institute, "Photovoltaics Student Guide," 2013.

[6] U.S. Department of ENergy, "The History of Solar," Energy Efficiency and Renewable Energy, Washington D.C..

[7] J. Perlin, From Space to Earth: The Story of Solar Electricity, Ann Arbor: Harvard University Press, 2002.

[8] G. Masters, Renewable and Efficient Electric Power Systems, 2nd ed., John Wiley & Sons, 2013.

[9] A. Sproul, "Understanding the p-n Junction," Resources for the Secondary Science, 2007.

[10] S. Wenham, M. Green, M. Watt and R. Corkish, Applied Photovoltaics, Sterline, Virginia: Routledge, 2011.

[11] A. Pradhan, D. S. Ali and C. Jena, "Analysis of Solar PV Cell Performance with Changing Irradiance and Temperature," *International Journal Of Engineering And Computer Science,* vol. 2, no. 1, pp. 214-220, January 2013.

[12] A. Parretta, M. Bombace, G. Graditi and R. Schioppo, "Optical Degradation of Field Aged C-Si Photovoltaic Modules," *Solar Energy Materials & Solar Cells,* vol. 86, pp. 349-364, 2005.

[13] D. C. Jordan and S. R. Kurtz, "Photovoltaic Degradation Rates - An Analytical Review," *Progress in Photovoltaics: Research and Applications,* June 2012.

[14] R. Ramaprabha and B. L. Mathur, "Impact of Partial Shading on Solar PV Module Containing Series Connected Cells," *International Journal of Recent Trends in Engineering,* vol. 2, no. 7, pp. 56-60, November 2009.

[15] B. Marion, J. Adelstein and K. Boyle, "Performance Parameters for Grid-Connected PV Systems," 2005.

[16] Solar Energy Industries Association, Greentech Media Inc, "U.S. Solar Market Insight," 2012.

[17] National Renewable Energy Lab, "Best Research-Cell Efficiencies," 2013.

[18] A. Luque and S. Hegedus, Handbook of Photovoltaic Science and Engineering, John Wiley & Sons, LTD, 2011.

[19] International Renewable Energy Agency, "Solar Photovoltaics," *Renewable Energy Technologies: Cost Analysis Series*, vol. 1, no. 4, June 2012.

[20] T. Saga, "Advances in Crystalline Silicon Solar Cell Technology for Industrial Mass Production," *NPG Asia Materials*, vol. 2, no. 3, pp. 96-102, July 2010.

[21] 6W Research, "Thin Film PV Market (2011-2016): Global Market Forecast," Business Wire, New York, 2011.

[22] J. Poortmans and V. Arkhipov, Thin Film Solar Cells: Fabrication, Characterization and Applications, Belgium: John Wiley & Sons, Ltd, 2006.

[23] H. Ullal, "Overview and Challenges of Thin Film Solar Electric Technologies," in *World Renewable Energy Congress X and Exhibition*, Glasgow, 2013.

[24] T. Markvart and L. Castaner, Practical Handbook of Photovoltaics Fundamentals and Applications, Elsevier, 2003.

[25] W. Bower, "International Guideline for the Certification of Photovoltaic System Components and Grid-Connected Systems," Internation Energy Association, Paris, 2002.

[26] L. Arribas, "World-Wide Overview of Design and Simulation Tools for Hybrid PV Systems," International Energy Agency, 2011.

[27] G. Klise and J. Stein, "Models Used to Assess the Performance of Photovoltaic Systems," Sandia National Laboratories, Albuquerque, 2009.

[28] “Modeling Tools,” National Renewable Energy Lab, [Online]. Available: http://www.nrel.gov/international/tools/fate-2hpt.

[29] “RETscreen International,” [Online]. Available: http://www.retscreen.net/.

[30] “HOMER Energy,” [Online]. Available: http://www.homerenergy.com/.

[31] “Energy Research Centre,” University of Cape Town, [Online]. Available: http://www.erc.uct.ac.za/hybrid-deisgner.

[32] “PVSYST Photovoltaic Software,” [Online]. Available: http://www.pvsyst.com/en/.

[33] Solar Energy Industries Association, Greentech Media Inc , “U.S. Solar Market Insight,” 2014.

[34] M. Platzer, "U.S. Solar Photovoltaic Manufacturing: Industry Trends, Global Competition, Federal Support," Congressional Research Service, 2012.

[35] R. Ramesh, "Sunshot Vision Study," Washington D.C., 2012.

[36] E. Holt and L. Bird, "Emerging Markets for Renewable Energy Certificates: Opportunities and Challenges," National Renwable Energy Lab, Golden, 2005.

[37] K. Cory, J. Coughlin and C. Coggeshall, "Solar Photovoltaic Financing: Deployment on Public Property by State and Local Governments," National Renewable Energy Lab, Golden, 2008.

[38] U.S. Department of Energy, North Carolina Solar Center, "Database of State Incentives for Renewables & Efficiency," U.S. Department of Energy, North Carolina Solar Center, Interstate Renewable Energy Council, Energy Efficiency & Renewable Energy, 2014. [Online]. Available: http://www.dsireusa.org/. [Accessed February 2014].

[39] P. Glasserman, Monte Carlo Methods in Financial Engineering, New York: Springer, 2003.

[40] A. Goodrich, T. James and M. Woodhouse, "Residential, Commercial, and Utility-Scale Photovoltaic (PV) System Prices in the United States: Current Drivers and Cost-Reduction Opportunities," National Renewable Energy Lab, 2012.

[41] MathWorks, *MATLAB.*

[42] *Image Magick,* 1999.

[43] L. Shapiro and G. Stockman, Computer Vision, Upper Saddle River, New Jersey: Prentice Hall, 2001.

[44] R. Gonzalel, R. E. Woods and S. L. Eddins, Digital Image Processing Using MATLAB, 2nd ed., Gatesmark Publishing, 2009.

[45] R. Ramabadran and B. Mathur, "Effect of Shading on Series and Parallel Connected Solar PV Modules," *Modern Applied Science,* 2009.

[46] A. J. Marsh, "Why Do Shading Calculations Take so Long?," *Natural Frequency Journal,* no. 4, November 2007.

[47] D. J. Luchini Colbry, *Human Face Verification by Robust 3D Surface,* Michigan State University: ProQuest, UMI Dissertations Publishing, 2006.

[48] N.-E. Yang, J. W. Lee and R.-H. Park, "Depth Map Generation Using Local Depth Hypothesis for 2D-To-3D Conversion," *International Journal of Computer Graphics & Animation,* vol. 3, no. 1, January 2013.

[49] W. Huang and K. He, “A New Heuristic Algorithm for Cuboids Packing with No Orientation Constraint,” *Computers and Operations Research,* no. 36, pp. 425-432, 2009.

[50] D. S. Liu, S. Y. Huang and S. K. Goh, “A Two-Dimensional Bin Packing Problem with Size Changeable Items for the Production of Wind Turbine Flanges,” *European Journal of Operational*

Research, no. 190, pp. 357-382, 2008.

[51] A. Pasha, “Geometric Bin Packing Algorithm for Arbitrary Shapes,” Gainesville, 2003.

[52] Y.-P. Chang, “Optimal The Tilt Angle for Photovoltaic Modules Using PSO Method with Nonlinear Time-Varying Evolution,” *Energy,* no. 35, pp. 1954-1963, 2010.

[53] J. D. Mondol, Y. Yohanis and B. Norton, “Optimal Sizing of Array and Inverter for Grid-Connect Photovoltaic Systems,” *Solar Energy,* no. 80, pp. 1517-1539, 2006.

[54] K. Kalaitzakis and G. Stavrakakis, “Size Optimization of a PV System Installed Close to Sun Obstacles,” *Pergamon,* vol. 57, no. 4, pp. 291-299, 1996.

[55] H. Tian and F. Mancilla-David, “Determination of Optimal Configuration for a Photovoltaic Array Depending on the Shading Condition,” *Solar Energy,* no. 95, pp. 1-12, 2013.

[56] T. Khatib, “Optimization of a Grid-Connected Renewable Energy System for a Case Study in Nablus, Palestine,” *International Journal of Low-Carbon Technologies,* March 2013.

[57] A. Dobos, "PVWatts Version 1 Technical Reference," National Renewable Energy Laboratory, Golden, 2013.

[58] H. Haeberlin, "Optimum DC operating Voltage for Grid-Connected PV Plants: Chose of Vmpp for Measurement of Efficiency and Vmpp-stc at PV Plants for Grid-Connected Inverters with a Wide DC Input Voltage Range," in *20th European Photovoltaic Solar Energy Conference*, Barcelona, 2005.

[59] National Electric Code, 52 ed., Quincy, Massachusetts: National Fire Protection Agency, 2011.

[60] D. King, W. Boyson and J. Kratochvil, "Photovoltaic Array Performance Model," Sandia National Laboratories, Albuquerque, 2004.

[61] Black & Veatch, "Cost and Performance Data for Power Generation Technologies," Black & Veatch, Overland Park, 2012.

[62] A. Williams, B. Atkinson and K. Garbesi, "Lighting Contols in Commercial Buildings," *Leukos,* vol. 8, no. 3, pp. 161-180, January 2012.

[63] D. DiLaura, K. Houser, R. Mistrick and G. Steffy, The Lighting Handbook, Illuminating Engineering Society, 2011.

[64] Lawrence Berkeley National Laboratory, Lighting Retrofit Handbook, Seattle, Washington: The U.S. Department of Energy: Federal Energy Management Program, 2001.

[65] J. Kesselring, "Lighting Retrofit Manual," Palo Alto, 1998.

[66] J. Snyder, "Light Sources and Color," *Lighting Research Center,* vol. 8, no. 1, October 2004.

[67] C. Eley, T. M. Tolen, J. R. Benya, F. Rubinstein and R. Verderber, "Advanced Lighting Guidelines,"

Eley Associates, Pleasant Hill, 1993.

[68] ASHRAE, ANSI and IESNA, Energy Standard for Buildings Expect Low-Rise Residential Buildings, 2012.

[69] Illuminating Engineering Society of North America, *Lighting Power Density (LPD) Public User's Manual*, 2005.

[70] M. Ashe, D. Chwastyk, C. d. Monasterio, M. Gupta and M. Pegors, "2010 U.S. Lighting Market Characterization," U.S. Department of Energy, 2012.

[71] Michigan State University, "Energy Conservation and Optimization Measures at Michigan State University," East Lansing, 2012.

[72] "Illuminating Engineering Society," 2012. [Online]. Available: http://www.ies.org/pdf/publicpolicy/DOE-Office-of-Hearings-and-Appeals-Approves-T8-Fluorescent-Lamp-Exception.pdf.

[73] United States Environmental Protection Agency, "Clean Energy," [Online]. Available: http://www.epa.gov/cleanenergy/energy-resources/refs.html. [Accessed February 2013].

[74] K. Ardani and R. Margolis, "2010 Solar Technologies Market Report," U.S. Department of Energy, Golden, 2011.

[75] P. Boyce, "The Impact of Light in Buildings on Human Health," *Indoor and Built Environment*, 2010.

[76] "Lighting Technologies: A Guide to Energy-Efficient Illumination," U.S. Environmental Protection Agency, Washington D.C..

[77] "Illuminating Engineering Society," 2011. [Online]. Available: http://www.ies.org/LDA/E-newsletter/2012/April/newswire/2012_04-nema.cfm. [Accessed 2013].

[78] "Information on Compact Fluorescent Light Bulbs (CFLs) and Mercury," 2010.

[79] M. Krarti, Energy Audit of Building Systems, vol. II, F. Kreith, Ed., Boca Raton, Florida: Taylor & Francis Group, 2011.

[80] M. Yamada and D. Chwastyk, "Adoption of Light-Emitting Diodes in Common Lighting Applications," Department of Energy, 2013.

[81] S. Broverman, Mathematics of Investment and Credit, 5 ed., ACETEX Academic Series, 2010.